ACS Chemical Neuroscience

pubs.acs.org/chemneuro Research Article

A Mechanism for the Inhibition of Tau Neurotoxicity: Studies with Artificial Membranes, Isolated Mitochondria, and Intact Cells

Segev Naveh Tassa, Shani Ben Zichri, Shiran Lacham-Hartman, Ofek Oren, Zeev Slobodnik, Ekaterina Eremenko, Debra Toiber, Raz Jelinek, and Niv Papo*

Cite This: *ACS Chem. Neurosci.* 2021, 12, 1563−1577 Read Online

ACCESS | Metrics & More | Article Recommendations | Supporting Information

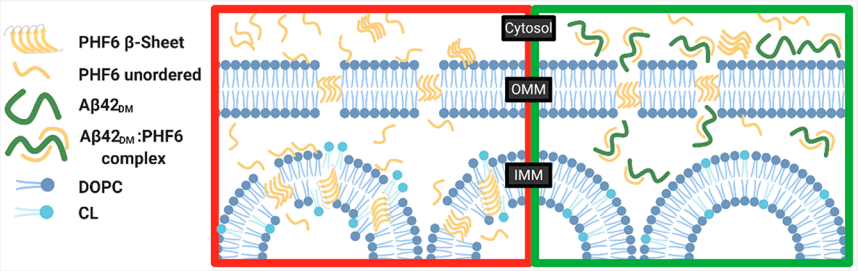

ABSTRACT: It is currently believed that molecular agents that specifically bind to and neutralize the toxic proteins/peptides, amyloid β (Aβ42), tau, and the tau-derived peptide PHF6, hold the key to attenuating the progression of Alzheimer's disease (AD). We thus tested our previously developed nonaggregating Aβ42 double mutant (Aβ42$_{DM}$) as a multispecific binder for three AD-associated molecules, wild-type Aβ42, the tau$_{K174Q}$ mutant, and a synthetic PHF6 peptide. Aβ42$_{DM}$ acted as a functional inhibitor of these molecules in *in vitro* assays and in neuronal cell-based models of AD. The double mutant bound both cytotoxic tau$_{K174Q}$ and synthetic PHF6 and protected neuronal cells from the accumulation of tau in cell lysates and mitochondria. Aβ42$_{DM}$ also reduced toxic intracellular levels of calcium and the overall cell toxicity induced by overexpressed tau, synthetic PHF6, Aβ42, or a combination of PHF6and Aβ42. Aβ42$_{DM}$ inhibited PHF6-induced overall mitochondrial dysfunction: In particular, Aβ42$_{DM}$ inhibited PHF6-induced damage to submitochondrial particles (SMPs) and suppressed PHF6-induced elevation of the ζ-potential of inverted SMPs (proxy for the inner mitochondrial membrane, IMM). PHF6 reduced the lipid fluidity of cardiolipin/DOPC vesicles (that mimic the IMM) but not DOPC (which mimics the outer mitochondrial membrane), and this effect was inhibited by Aβ42$_{DM}$. This inhibition may be explained by the conformational changes in PHF6 induced by Aβ42$_{DM}$ in solution and in membrane mimetics. On this basis, the paper presents a mechanistic explanation for the inhibitory activity of Aβ42$_{DM}$ against Aβ42- and tau-induced membrane permeability and cell toxicity and provides confirmatory evidence for its protective function in neuronal cells.

KEYWORDS: *Tau, PHF6, Aβ42, Alzheimer's disease, amyloids, neurodegeneration*

INTRODUCTION

Dementia is becoming a major health burden for most societies, reflecting their aging populations. According to the World Alzheimer Report,[1] over 50 million cases of Alzheimer's disease (AD) were recorded worldwide in 2019, and that number is expected at least to double by 2050. Nonetheless, despite intensive R&D efforts, current treatments for AD and related forms of dementia are limited, and a cure remains elusive.

Two signature protein deposits are commonly found in the AD brain, namely, plaques comprising amyloid-β (Aβ) peptide aggregates and fibrils, and neurofibrillary tangles (NFTs) assembled mostly from hyperphosphorylated or acetylated tau.[2] The Aβ peptides (36−43 residue protein segments) are formed on the plasma membrane of neuronal cells[3] and on the membranes of intracellular organelles by cleavage of the transmembrane amyloid precursor protein (APP) by β- and γ-secretases. The resulting monomeric Aβ cleavage products are then released into the extracellular matrix from the plasma cell membrane or into the cytosol from the membranes of intracellular organelles.[4] In these milieus, the disordered Aβ monomers assume a β-sheet conformation,[5] initiating an oligomerization/fibrillation pathway that proceeds from Aβ cleavage product monomers through oligomers to fibrils and plaques. Oligomers, plaques, and fibrils containing amyloid-β1−42 (Aβ42, the toxic 42-residue fragment of Aβ) have been shown to modulate, to different extents, intracellular calcium

Received: January 25, 2021
Accepted: April 19, 2021
Published: April 27, 2021

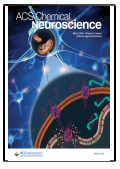

https://doi.org/10.1021/acschemneuro.1c00045
ACS Chem. Neurosci. 2021, 12, 1563−1577

levels, mitochondrial activity, and neuronal cell toxicity.[6−9] It is generally held that it is the Aβ oligomers that are the species responsible for the neurotoxicity (i.e., loss of synapses and disintegration of the neuronal network[10]) of Aβ, whereas Aβ fibrils are considered less neurotoxic, despite their abundance in the AD brain. Nevertheless, the toxicity mechanism is still subject to debate, and the toxic species have still not been pinpointed definitively, despite ongoing studies in many laboratories.[11]

The other signature protein, tau, a member of the microtubule-associated protein (MAP) family,[12] is concentrated primarily in the axons of neurons.[12] There are six tau isoforms in the human brain, each comprising 352−441 amino acids[12] and containing 3 or 4 conserved tubulin-binding motifs, namely, R1, R2, R3, and R4 (amino acids 244−274, 275−305, 306−336, and 337−378, respectively), all located toward the carboxy terminus of tau (Figure S1). A variety of loss-of-function mutations result in enhanced tau phosphorylation and acetylation,[13,14] leading to dissociation of the functionalized proteins from the microtubules and their accumulation in the cytosol. The increased concentration facilitates tau homodimerization, followed by nucleation, oligomerization, and (once the critical nucleus cluster size is reached) accumulation as straight filaments (SFs) or paired helical filaments (PHFs).[15,16] These filaments then cluster further to form NFTs,[16] leading to toxic effects.[2,17] Mutated tau self-assembles via its R3 and R4 repeats that form the hydrophobic core of the SFs and PHFs, a process that is dependent on a unique conserved tubulin-binding motif within the R3 repeat, namely, ^{306}VQIVYK^{311}, also known as PHF6, which is highly amyloidogenic[18] and has a β-sheet structure similar to the structure formed in the core of the tau fibril[2,19−22] (Figure S1). PHF6 is thus used in many studies as a model for the mechanism of action and the toxic effects of tau, as is done in this study.

In light of the above, there is currently a realization (supported by a string of failures in the search for a treatment for AD) that a potent therapeutic will probably be one that targets both Aβ42 and tau.[23] Indeed, despite promising preclinical and phase 2 clinical studies, nonpeptidic first-generation treatments targeting Aβ aggregation have not been successful.[23,24] Similarly, the tau-targeting short-chain fatty acid valproate gave disappointing results in phase 3 clinical trials, with no changes in cognitive and functional status of AD patients.[23,25] The idea of targeting both Aβ42 and tau has received support from animal studies and clinical trials of the neuroprotective short peptide NAP (NAPVSIPQ, davunetide, CP201), which was originally developed to enhance the association between tau and microtubules.[26,27] In animal models of AD, NAP showed potency in both inhibiting tauopathy and abolishing Aβ42 toxicity. NAP also had a positive effect on cognition in phase 2 trials of patients with amnestic mild cognitive impairment and was shown to be safe and well tolerated.[26]

The idea of developing a potent therapeutic that targets both Aβ42 and tau has been given further credence by studies showing that there is significant crosstalk between Aβ42 and tau,[28,29] with three possible modes of interaction between the two. In the first, Aβ42 drives tau pathology; e.g., intracranial injection of synthetic Aβ42 into mutant tau transgenic mice escalated NFT pathology,[30] and Aβ42 plaques accelerated tau expression and cognitive decline in human AD.[31,32] In the second interaction mode, tau mediates Aβ toxicity; e.g., tau knockout *in vivo* prevented Aβ-induced defects in the axonal transport of intracellular cargoes and mitochondria.[33] The third mode involves the synergistic toxic effects of Aβ42 and tau: In causing downstream toxicity, Aβ and tau target different components of the same pathway, amplifying one another's toxic effects.[34] The interaction between Aβ42 and tau is also manifested in an elevation of intracellular calcium.[35,36] In the AD synapse, tau activates the inositol trisphosphate receptor (IP3), which results in an increased release of calcium from the endoplasmic reticulum into the cytoplasm.[17] Aβ42 causes the same effect of intracellular calcium elevation by permeating the plasma membrane and forming calcium-permeable membrane pores that facilitate calcium internalization from the extracellular space into the cytoplasm.[37]

A number of studies have shown that the Aβ42−tau toxicity cascade starts with mitochondrial disruption, with the two proteins permeating through the outer mitochondrial membrane (OMM) and disrupting the inner mitochondrial membrane (IMM), but only very few have examined disruption of the IMM by PHF6. In attempts to mimic these interactions in the laboratory, most studies model the OMM and IMM as large and small unilamellar vesicles (LUVs and SUVs, respectively) by using zwitterionic 2-dioleoyl-*sn*-glycero-3-phosphocholine (DOPC)[5,38] and DOPC/anionic cardiolipin (CL),[38,39] respectively. It is known that tau and Aβ42 share common characteristics upon their interaction with phosphatidylcholine (PC) phospholipid bilayers[19,20] that mimic the OMM (due to an approximate abundance of 40% of PC in all plasma membrane lipids), with both proteins forming β-sheet rich nanopores and, later on, more mature β-sheet-rich fibrillary structures.[5,38,40] It is also known that tau[41] and Aβ42[5,38] interact with DOPC to form transiently stable oligomeric structures and that both proteins can also interact with CL, which is found exclusively in the IMM.[39] In fact, the interaction of both tau and Aβ42 with CL in cells is a prerequisite for tau and Aβ42 to dissociate from the OMM and interact with the IMM and for the two proteins to induce mitochondrial membrane perturbation.[38,42] Despite the abilities of both Aβ42 and tau to interact with both PC and CL, their modes of interaction with these two lipids are different, but the bases for this difference and its effect on cell toxicity are yet to be determined.[19,43] In addition, it is known that both proteins interact preferentially with anionic phospholipids.[40,44] Nevertheless, the interaction of tau with the anionic CL that mimics the IMM has been explored only marginally.[42]

From the above, it is evident that tau and Aβ42 exhibit mechanistic similarity with regard to the underlying molecular mechanisms of AD pathology. In addition, they have been shown to interact with one another in cell cultures and in the brain cells of AD patients,[32,34] with the interaction, which is stabilized by both hydrophobic interactions and electrostatic forces,[45] being based on the similar β-sheet-based fibril structures adopted by the two proteins[18,46] within the mitochondrial membranes,[19,38,42] resulting in a reduction in mitochondrial activity[34] and intracellular calcium elevation.[6,17] Since both tau and Aβ42 target the same phospholipids in the mitochondria and since their interactions with these phospholipids appear to lead to neuronal dysfunction and cell death, it would be reasonable to assume (although yet to be demonstrated) that the effect of the proteins acting in concert on the mitochondrial membranes and/or the neurons would be synergistic.[2,47] We therefore sought to test, in the

https://doi.org/10.1021/acschemneuro.1c00045
ACS Chem. Neurosci. 2021, 12, 1563−1577

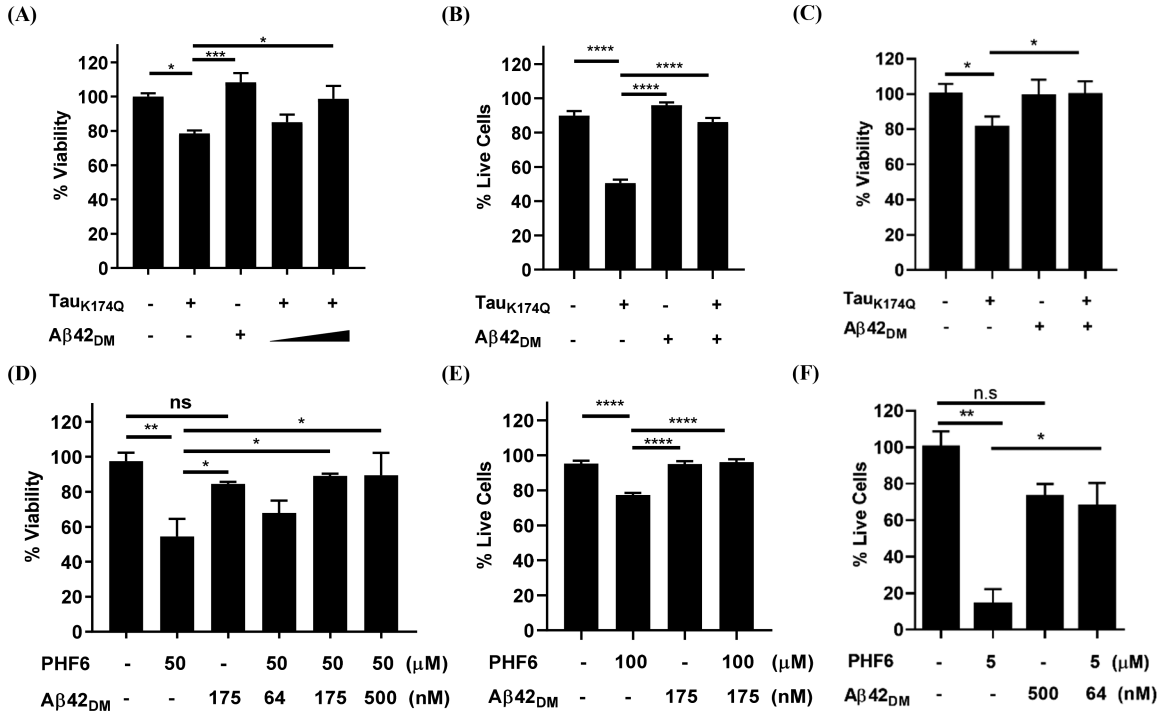

Figure 1. Aβ42$_{DM}$ reduces tau$_{K174Q}$- and PHF6-induced toxicity in cells. (A, B) SH-SY5Y cells transiently expressing tau$_{K174Q}$, Aβ42$_{DM}$, or both at tau$_{K174Q}$:Aβ42$_{DM}$ ratios of 2:1 (A) or 1:1 (A and B). (C) Primary cortical culture infected with tau$_{K174Q}$, Aβ42$_{DM}$, or both. (D, E) SH-SY5Y and (F) primary cortical cells treated extracellularly for 48 h with synthetic PHF6, Aβ42$_{DM}$, or both at different concentrations. Cell viability was determined using XTT (A, C, D), live cell count (B, E), or crystal violet staining (F) assays. Results are shown as percent of control. Comparison of mean cell viability values (n = 3) was performed by ANOVA test: *, $P < 0.1$; **, $P < 0.05$; ***, $P < 0.01$; ****, $P < 0.001$; error bars indicate the standard error of independent experiments performed in triplicate.

study reported here, a strategy that would simultaneously target both proteins by interfering with their ability to form stable β-sheet conformations, to oligomerize/self-aggregate, to interact with one another, and to interact with membrane phospholipids. Our novel strategy is based on using a multispecific Aβ42-based inhibitor that targets both the Aβ42/tau interaction and the interactions of the two proteins with the mitochondrial membranes, especially the IMM. In this study, we exploit our previously developed Aβ42 variant carrying two mutations, F19S and L34P (designated Aβ42$_{DM}$), that does not form a β-sheet structure in solution.[48] This double mutant (previously shown to abolish Aβ40 toxicity by disrupting the F19-L34 contact and drastically reducing the mutant's affinity for the cell membrane[49,50]) acts as an inhibitor that targets both tau and Aβ42, inhibiting their self-aggregation, interaction, and toxicity to neuronal cells. We show here that Aβ42$_{DM}$ binds both to the tau proxy, PHF6, and to Aβ42 and in so doing exhibits synergistic activity (vs targeting each protein separately) in inhibiting their accumulation in cells, their aggregation, their interaction with the IMM, and mitochondrial membrane disruption and hence also tau- and Aβ-induced neuronal cell death.

RESULTS AND DISCUSSION

Aβ42$_{DM}$ Inhibits Cell Toxicity Induced by Tau$_{K174Q}$ Overexpression and by Treatment with PHF6. SH-SY5Y neuroblastoma and mouse primary cortical cells intracellularly expressing both Aβ42$_{DM}$ and the loss-of-function tau mutant, tau$_{K174Q}$ (Figure S1), exhibited reduced toxicity vs cells that do not express Aβ42$_{DM}$ (Figure 1A–C). Similarly, SH-SY5Y and primary cortical cells treated extracellularly with Aβ42$_{DM}$ and a synthetic Ac-PHF6-NH$_3$ peptide (a tau-derived peptide mimetic,[51,52] hereinafter referred to as synthetic PHF6) also exhibited reduced toxicity vs cells that were not treated with Aβ42$_{DM}$ (Figure 1D–F). These results were obtained using XTT (Figure 1A,C,D), live cell count (Figure 1B,E), and crystal violet staining (Figure 1F) assays, with the XTT results showing a dose-dependent inhibitory effect by Aβ42$_{DM}$.

Aβ42$_{DM}$ Reduces Tau$_{K174Q}$ Accumulation in a Cell Lysate and in Mitochondria. In light of the above findings, we tested whether inhibition of cell death by Aβ42$_{DM}$ is the result of the inhibition of tau$_{K174Q}$ accumulation in the cells. Aβ42$_{DM}$ overexpressed in SH-SY5Y cells showed a dose-dependent effect in reducing the accumulation of overexpressed Flag-tau$_{K174Q}$-GFP. This inhibitory effect was observed both in the cell lysate (Figure 2A) and in isolated mitochondria (Figure 2B), with different fragments of tau$_{K174Q}$ being inhibited by Aβ42$_{DM}$ in the two different cell fractions. In the whole cell lysate, there was a decrease mainly in the 75 kDa fraction of monomeric tau$_{K174Q}$. The mitochondrial lysate also showed a decrease in tau$_{K174Q}$ accumulation but with the main cleavage product having a size of ~37 kDa, a product that has not yet been identified in previous studies.[53]

Aβ42$_{DM}$ Interacts with Cellular Tau$_{K174Q}$ and PHF6. Having demonstrated that Aβ42$_{DM}$ effectively inhibits tau$_{K174Q}$ accumulation in SH-SY5Y cells, we went on to show, in coimmunoprecipitation experiments, that the two proteins Aβ42$_{DM}$ and tau$_{K174Q}$ form a complex in these cells (Figure 2C). To explore the complex formation in greater depth and to elucidate the molecular mechanism of tau inhibition by Aβ42$_{DM}$, all subsequent experiments were performed with

https://doi.org/10.1021/acschemneuro.1c00045
ACS Chem. Neurosci. 2021, 12, 1563–1577

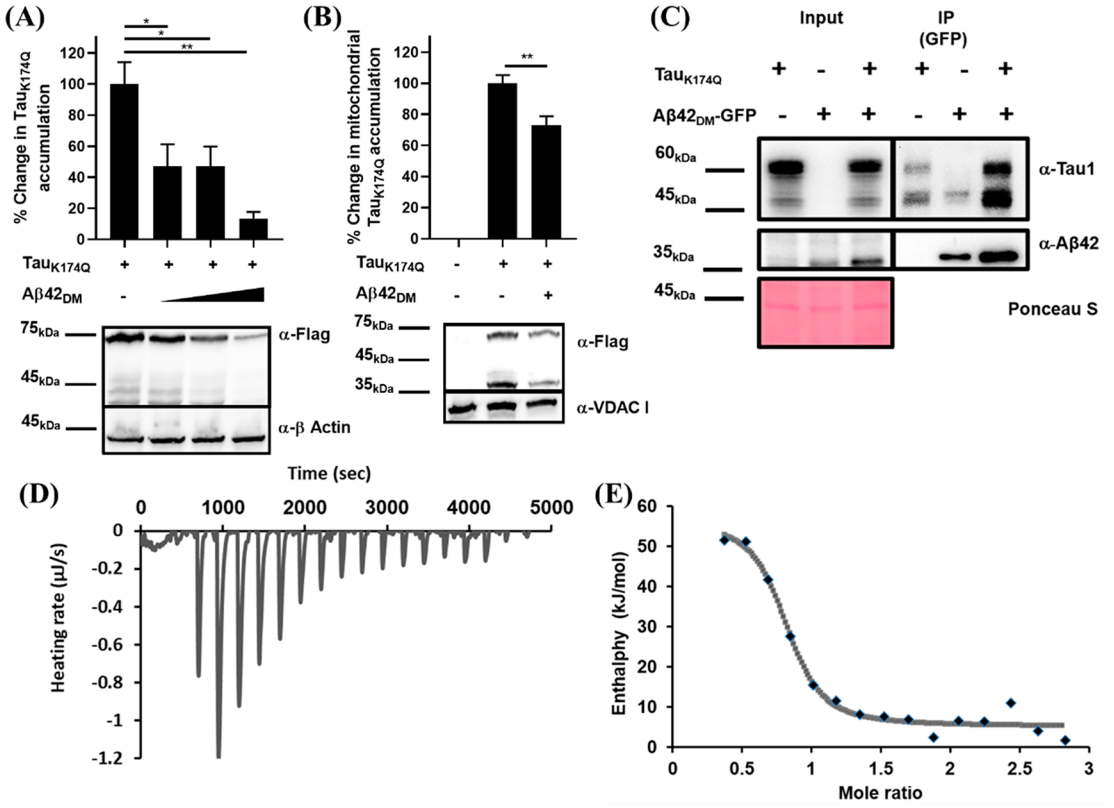

Figure 2. Aβ42$_{DM}$ interacts with tau$_{K174Q}$ to reduce the accumulation of tau$_{K174Q}$ in SH-5YSY cells. (A) Western blot analysis of SH-5YSY cell lysate overexpressing (for 48 h) Flag-tau$_{K174Q}$, Aβ42$_{DM}$, or combinations of two at Flag-tau$_{K174Q}$:Aβ42$_{DM}$ ratios of 2:1, 1:1, and 1:2. Empty plasmid was used as the control, and staining for β-actin expression was used for quantification. (B) Same experiment as in panel A but for a mitochondrial lysate. Staining for VDAC-I expression was used for quantification. (C) SH-5YSY cells transiently expressing tau$_{K174Q}$, Aβ42$_{DM}$-GFP, or both (in 1:1 ratio) were lysed and subjected to immunoprecipitation with protein G (which binds to anti-GFP antibody) conjugated to magnetic beads, followed by staining with an anti-GFP antibody. Ponceau S staining was used for normalization to total protein quantities. (D) ITC thermogram showing the Aβ42$_{DM}$−PHF6 binding interaction. (E) Affinity titration curve showing the enthalpy changes with increasing PHF6:Aβ42$_{DM}$ molar ratio.

synthetic PHF6 as a model for tau, since hydrophobic interactions between Aβ42 and PHF6 are believed to be responsible for tau−Aβ42 interactions[54] (Figure S1).

To test whether Aβ42$_{DM}$ and synthetic PHF6 interact directly, isothermal titration calorimetry (ITC) was performed. The binding titration profile and the thermodynamic interaction parameters [Gibbs free energy (ΔG), enthalpy (ΔH), and entropy (ΔS)] are shown in Figure 2D,E and Table 1. The negative ΔG value (−34.14 kJ·mol^{-1}) indicates a spontaneous interaction between Aβ42$_{DM}$ and synthetic PHF6, and the positive values obtained for ΔH (51.21 kJ·mol^{-1}) and $T\Delta S$ (85.3 kJ·mol^{-1}) at 25 °C provide confirmation of the hydrophobic nature of the interaction. The value of the entropy term $T\Delta S$ is ∼2-fold higher than the value of ΔH, suggesting that the interactions between Aβ42$_{DM}$ and synthetic PHF6 are "entropy-driven" rather than "enthalpy-driven". This set of experiments also included determination of the binding constant (K_d) for the Aβ42$_{DM}$−synthetic PHF6 complex; the obtained value of 1.03 ± 0.82 μM is within the range previously determined for complexes of PHF6 with other known inhibitors.[21,55] The stoichiometric ratio (n = 0.763, Table 1) may indicate that a single Aβ42$_{DM}$ molecule interacts with ∼2 monomers of PHF6, which suggests that binding of Aβ42$_{DM}$ to PHF6 begins at a very early stage of PHF6 oligomerization, before the latter becomes a fibril.

Table 1. Thermodynamic Parameters for the Binding between Aβ42$_{DM}$ and PHF6, As Determined from Isothermal Titration Calorimetry (ITC) Measurements

parameter	value
K_d (M)	(1.03 ± 0.82) × 10^{-6}
n	0.763 ± 0.053
ΔH (kJ·mol^{-1})	51.21 ± 6.39
ΔS (kJ·mol^{-1}·K^{-1})	286.4 × 10^{-3}
ΔG (kJ·mol^{-1})	−34.14 ± 6.39

Aβ42$_{DM}$ Reduces PHF6-Induced Enhancement in Intracellular Calcium Levels. In an experiment to examine whether Aβ42$_{DM}$ could inhibit the tau-induced enhancement in intracellular calcium levels in SH-SY5Y cells,[36] synthetic PHF6 was used as a model for the full-length tau. We thus followed the intracellular calcium levels upon treatment of SH-SY5Y cells with synthetic PHF6, Aβ42$_{DM}$, or both. Treatment with synthetic PHF6 enhanced intracellular calcium levels in a dose-dependent manner (Figure 3A). However, when the cells were treated with a mixture of Aβ42$_{DM}$ and synthetic PHF6 (at a molar ratio of 1:286, the same ratio used in the cell toxicity assays), the PHF6-mediated intracellular calcium level elevation was suppressed and returned to control levels. Treating the cells with Aβ42$_{DM}$ alone resulted in a small but nonsignificant enhancement in intracellular calcium levels, which may be explained by the fact that Aβ42$_{DM}$ is a Aβ42

https://doi.org/10.1021/acschemneuro.1c00045
ACS Chem. Neurosci. 2021, 12, 1563−1577

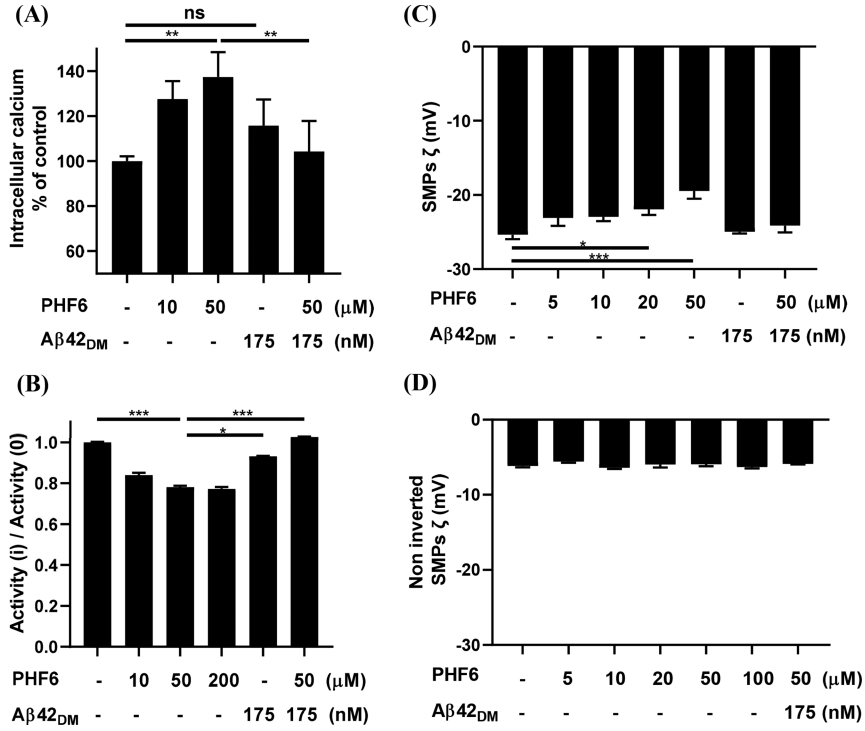

Figure 3. Aβ42$_{DM}$ inhibits PHF6-induced intracellular effects on cells and submitochondrial particles (SMPs). (A) Aβ42$_{DM}$ suppresses the synthetic PHF6-mediated elevation in intracellular calcium levels in SH-SY5Y cells. The cells were incubated with Aβ42$_{DM}$ alone or with preformed synthetic PHF6 aggregates in the presence or absence of Aβ42$_{DM}$. Calcium levels were determined by using a direct calcium assay (Fluo-4 direct assay kit). (B) Aβ42$_{DM}$ inhibits synthetic PHF6-induced reduction in COX activity. COX absorbance at 550 nm was measured after 24 h of incubation with a ferrocytochrome *c* solution (0.22 mM). (C) Aβ42$_{DM}$ suppresses the synthetic PHF6-induced elevation in the ζ-potential of inverted SMPs but (D) does not affect the ζ-potential of noninverted SMPs. SMPs were treated with synthetic PHF6 at different concentrations, Aβ42$_{DM}$ at 175 nM (panels A−C), or a combination of Aβ42$_{DM}$ and synthetic PHF6 at a molar ratio of 1:286. Statistical analysis (n = 3) was performed with an ANOVA test: *, $P < 0.1$; **, $P < 0.05$; ***, $P < 0.01$; ****, $P < 0.001$; error bars indicate the standard error of independent experiments performed in triplicate.

derivative, and Aβ42 has been shown in previous studies to cause an elevation in intracellular calcium levels.[38]

Aβ42$_{DM}$ Inhibits PHF6-Induced Damage in Isolated Mitochondrial Particles. Since tau-induced AD symptoms are related to enhanced cellular calcium levels[17] and hence to mitochondrial dysfunction,[42] we aimed to test whether synthetic PHF6 would also cause mitochondrial dysfunction. To this end, we isolated mitochondria from SH-SY5Y cells and formed inside-out submitochondrial particles (SMPs), in which the IMM is exposed to the medium, thereby enabling us to determine the activity of the IMM-located cytochrome *c* oxidase (COX), whose proper function[56] is crucial for the mitochondrial respiratory system.[57] We evaluated the changes in COX activity in the SMPs upon treatment with synthetic PHF6, Aβ42$_{DM}$, or a mixture of synthetic PHF6 and Aβ42$_{DM}$. Our results show that synthetic PHF6 reduced COX activity in a dose−response manner (Figures 3B and S2). Notably, a mixture of Aβ42$_{DM}$ and synthetic PHF6 at a molar ratio of 1:286 abolished the PHF6-induced reduction in COX activity.

Aβ42$_{DM}$ Suppresses the PHF6-Induced Elevation of the ζ Potential of Inverted SMPs. Mitochondrial dysfunction induced by Aβ42 and tau is mediated via their ability to disrupt both the IMM and the OMM.[6,39,40] We thus tested whether synthetic PHF6, as a model for tau, interferes with inner and outer mitochondrial membranes isolated from intact cells and whether Aβ42$_{DM}$ can inhibit PHF6-induced mitochondrial membrane disruption. To this end, a ζ-potential assay, which is indicative of membrane electrical charge and integrity,[58] was performed for inverted (i.e., IMM exposed to the medium, Figure 3C) and noninverted (i.e., OMM exposed to the medium, Figure 3D) SMPs treated with synthetic PHF6, Aβ42$_{DM}$, or a combination of the two peptides. Our results demonstrated that synthetic PHF6 disrupted the integrity of IMM (as shown by an elevated ζ-potential of the inverted SMPs) but not of OMM and, importantly, that Aβ42$_{DM}$ abolished the PHF6-mediated elevation of the ζ-potential of the inverted SMPs (at a molar ratio of Aβ42$_{DM}$:synthetic PHF6 of 1:286).

Aβ42$_{DM}$ Induces Conformational Changes in PHF6 in Solution and in Membrane Mimetics. With the aim to understand how Aβ42$_{DM}$ interferes with synthetic PHF6-induced mitochondrial membrane damage and the reason for the selective activity exhibited by synthetic PHF6 on the inner vs the outer mitochondrial membrane, we used a system of lipid vesicles that mimic the IMM or the OMM to follow the structural changes in synthetic PHF6 in the absence or presence of Aβ42$_{DM}$.[38,39,59] For quantification of the synthetic PHF6 β-sheet structure, we used a thioflavin T (ThT) fluorescence assay, which is based on the correlation between the binding of ThT to an amyloid-like peptide and its β-sheet content.[60] A significant reduction (~50%) in the ThT signal of synthetic PHF6 was obtained upon its interaction with Aβ42$_{DM}$ in the presence of heparin, which induces a β-sheet structure in PHF6[21,61] (Figure 4Ai), namely, a structure similar to that adopted by the PHF6 peptide when it is a part of the full-length tau fibril core.[18] As was to be expected, a ThT signal

https://doi.org/10.1021/acschemneuro.1c00045
ACS Chem. Neurosci. 2021, 12, 1563−1577

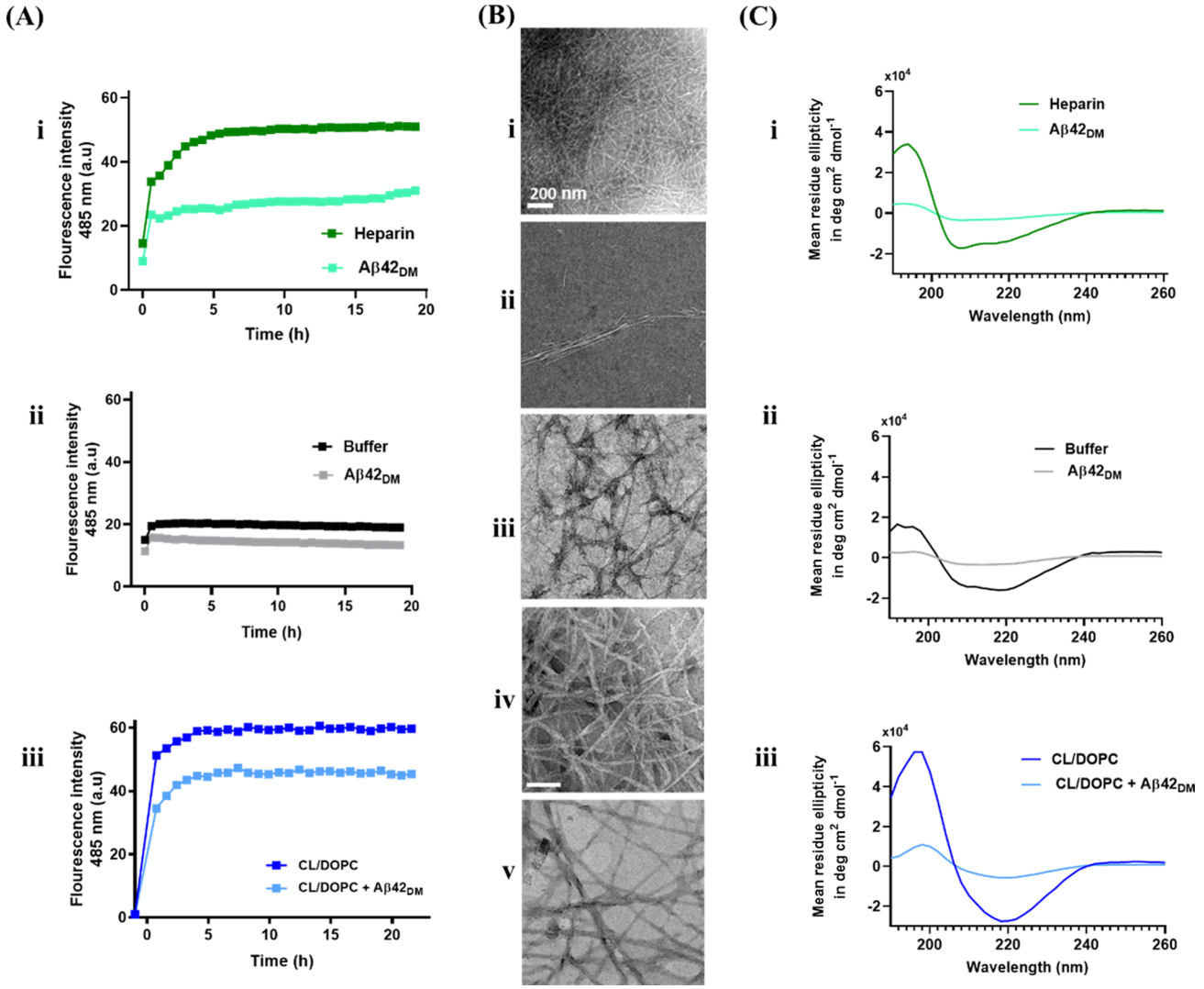

Figure 4. Aβ42$_{DM}$ disrupts the formation of a PHF6 β-sheet structure in heparin-supplemented sodium phosphate buffer, in buffer alone, and in CL/DOPC phospholipids. (A) ThT fluorescence was monitored over time upon co-incubation at 25 °C of synthetic PHF6 (50 μM) with Aβ42$_{DM}$ (175 nM) in the presence of heparin (Ai), sodium phosphate buffer (Aii), and CL/DOPC SUVs (Aiii). (B) TEM images taken 24 h after incubation of synthetic PHF6 and heparin (Bi); synthetic PHF6, heparin, and Aβ42$_{DM}$ (Bii); synthetic PHF6 in sodium phosphate buffer (Biii); synthetic PHF6 in CL/DOPC (Biv); and synthetic PHF6 and Aβ42$_{DM}$ in CL/DOPC (Bv). (C) Circular dichroism (CD) spectra of synthetic PHF6 (50 μM) in the absence or presence of Aβ42$_{DM}$ (175 nM) in heparin solution (Ci), sodium phosphate buffer (Cii), and CL/DOPC vesicles (Ciii). CD spectra were obtained at wavelength of 185−260 nm using a quartz cuvette with a path length of 1 mm. Samples were analyzed after 24 h of incubation in 10 mM sodium phosphate buffer.

for synthetic PHF6 was not observed in the absence of heparin (Figure 4Aii). The next step was therefore to test whether the structure of synthetic PHF6 actually changes when it interacts with phospholipids that mimic the IMM and OMM and whether Aβ42$_{DM}$ inhibits this change. To date, it is known only that PHF6 interacts with the IMM and OMM (either alone or as part of tau[41−43]) and that it forms stable β-sheet rich complexes with phospholipids that mimic the IMM and OMM,[41] thereby inducing membrane disruption[62] and interrupting lipid packing.[40] Indeed, a significant reduction (~25%) in the ThT signal was obtained upon interaction between synthetic PHF6 and Aβ42$_{DM}$ in the presence of CL/DOPC (a phospholipid composition that mimics the IMM but not the OMM[63,64]) (Figure 4Aiii) but not in the presence of DOPC (which mimics OMM phospholipids[39,65]) (Figure S3A). These findings indicate that synthetic PHF6 adopted a ThT-reactive β-sheet conformation in CL/DOPC (IMM) but not in DOPC (OMM) phospholipids and that in the former case the synthetic PHF6 β-sheet structure could be abolished by Aβ42$_{DM}$.

The above findings are in keeping with the results of TEM imaging, which showed that, in the presence of heparin, synthetic PHF6 adopted a densely packed, long, and uniform fibrillary conformation (Figure 4Bi). Upon treatment with Aβ42$_{DM}$, this fibril morphology was destroyed and a decrease in fibril density was observed (Figure 4Bii). For the control, untreated synthetic PHF6, dissolved in sodium phosphate buffer, showed fibrils that were significantly less densely packed (Figure 4Biii) than in the presence of heparin, in agreement with the ThT results. In the presence of CL/DOPC, thick, densely packed uniform synthetic PHF6 fibrils were obtained (Figure 4Biv), whereas treatment with Aβ42$_{DM}$ resulted in a significant decrease in fibril density (Figure 4Bv). In DOPC, it was found that undisrupted, intact DOPC vesicles coexisted

https://doi.org/10.1021/acschemneuro.1c00045
ACS Chem. Neurosci. 2021, 12, 1563−1577

with a small quantity of synthetic PHF6 fibrils, suggesting an interaction between the peptide and DOPC that differs from that for synthetic PHF6 and CL/DOPC phospholipids, i.e., synthetic PHF6 binds but does not disrupt DOPC vesicles, whereas it does disrupt CL/DOPC vesicles (Figure S3B).

The above findings were confirmed by CD spectroscopy, which followed structural changes in synthetic PHF6 at higher resolution than that possible with the ThT assay. The CD spectra showed that synthetic PHF6 adopts a mixture of helical and β structures (with minima at 208, 217, and 222 nm) when aggregated (in the presence of heparin, Figure 4Ci) and mostly helical structures (Figure 4Cii) when not aggregated (i.e., when dissolved in sodium phosphate buffer).[43,66] Here again, Aβ42$_{DM}$ reduced the CD signal significantly in both samples (heparin supplemented and buffer alone), which indicates a reduction of the synthetic PHF6 secondary structure[67] (Figure 4Ci,ii). Of note, synthetic PHF6 adopted a predominantly β-sheet structure (with a minimum at 217 nm) in the presence of CL/DOPC, and this structure was also lost upon addition of Aβ42$_{DM}$. The predominantly β-sheet structure of synthetic PHF6 explains its higher ThT reactivity in CL/DOPC vesicles in comparison to heparin-supplemented medium and buffer, with the latter showing a predominant α-helical structure. The fact that Aβ42$_{DM}$ abolished the β-sheet and fibrillary structures of synthetic PHF6 in CL/DOPC vesicles is also in agreement with the reduction of the ThT signal in the synthetic PHF6–CL/DOPC sample in the presence of Aβ42$_{DM}$.

PHF6 Reduces CL/DOPC, but Not DOPC or DOPG/DOPC, Lipid Fluidity and This Effect Is Inhibited by Aβ42$_{DM}$. To further determine the effect of synthetic PHF6 on the mitochondrial inner and outer membranes, the fluorescence anisotropy of 1,6-diphenyl-1,3,5-hexatriene (DPH) incorporated into CL/DOPC (10:90) or DOPC SUVs was determined. Monitoring the fluorescence anisotropy of DPH, which is embedded in the interior of the phospholipid bilayer (far from the fatty acid head groups),[68] allows us to probe, with high sensitivity, the fluidity and dynamics of the membrane lipid bilayer.[69] The results revealed that incubation of synthetic PHF6 with DPH-labeled CL/DOPC SUVs resulted in a dose-dependent enhancement in the anisotropy (Figure 5A), indicating reduced bilayer fluidity upon binding of synthetic PHF6 to the lipids.[70] This effect was abolished upon treatment with Aβ42$_{DM}$. Interestingly, synthetic PHF6 had no such effect on the fluidity of DPH-labeled DOPC (Figure 5B) or DOPC/DOPG (at 80:20 molar ratio) vesicles (Figure 5C), suggesting that while the presence of CL is obligatory for the disruption of lipid vesicles by PHF6, the presence of a negatively charged lipid is not a criterion for disruption (since there is the same amount of negative charge in the phospholipid compositions of the DOPC/CL and DOPC/DOPG SUVs used in our assay[71]). These results further confirm that the interaction of PHF6 with the IMM, but not with the OMM or the plasma membrane, is the cause of its intracellular effects that eventually lead to cell death.

Aβ42$_{DM}$ Inhibits the Cell Toxicity That Is Mediated by a Combination of PHF6 and Aβ42. The ability of tau or Aβ42 to drive neuronal dysfunction and neurodegeneration has been known for quite some time, but the synergistic toxicity between tau and Aβ42 was shown only recently.[47,72] Accordingly, we previously demonstrated the protective effect conferred by Aβ42$_{DM}$ in neuronal cells treated with Aβ42. Since a similar protective effect was observed in the Aβ42$_{DM}$-induced inhibition of tau and PHF6 toxicity, our next step was

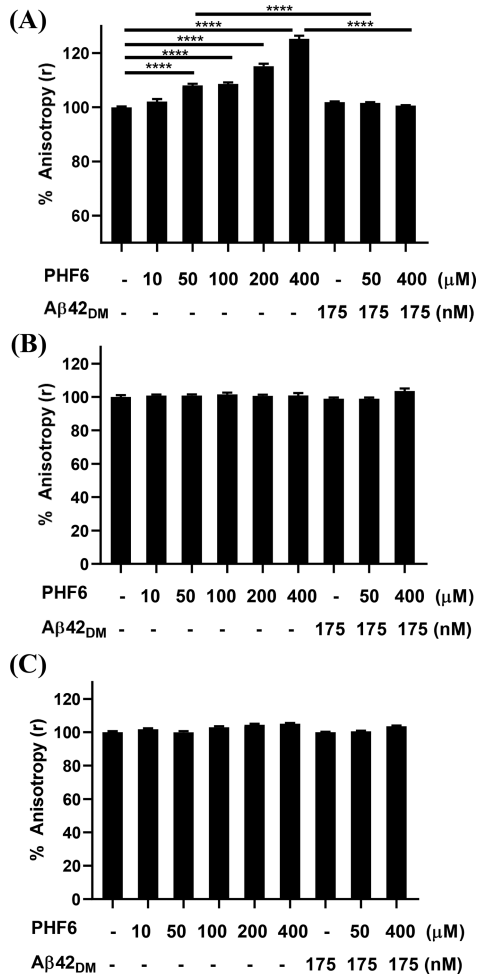

Figure 5. Aβ42$_{DM}$ inhibits the PHF6-mediated reduction in DOPC/CL membrane fluidity. Interactions of synthetic PHF6, Aβ42$_{DM}$, or a mixture of the two with phospholipid vesicles were measured by following bilayer dynamics using fluorescence anisotropy of DPH-labeled lipid vesicles. Shown are the fluorescence anisotropy values of DPH embedded in (A) DOPC/CL (90:10 molar ratio) vesicles, (B) DOPC vesicles, or (C) DOPC/DOPG (80:20 molar ratio) vesicles. Statistical analysis (n = 7) was performed with an ANOVA test: ****, P < 0.001; error bars indicate standard error.

thus to test whether a dual inhibitory effect could be obtained upon treatment with Aβ42$_{DM}$ of SH-SY5Y cells challenged with Aβ42 and synthetic PHF6 together. To this end, SH-SY5Y cells were incubated with synthetic PHF6 (50 μM), Aβ42 (10 μM), Aβ42$_{DM}$ (175 nM), or different mixtures of two or three of the peptides. For cell viability determination, an XTT assay was performed (Figure 6). Our results show that synthetic PHF6 reduced cell viability to ∼80%, Aβ42 reduced cell viability to ∼80%, and the two peptides together reduced cell viability to ∼70%. Excitingly, Aβ42$_{DM}$ treatment reversed the decrease in cell viability in all the treatments, suggesting a dual (against both Aβ42 and synthetic PHF6) protective effect.

In this study, we developed a new strategy in which Aβ42$_{DM}$, a nonaggregating Aβ42 double mutant, inhibits the neuronal cell toxicity induced by full-length tau$_{K174Q}$ and its derived neurotoxic peptide PHF6.[40,61] While Aβ42$_{DM}$ was previously developed in our laboratory to reduce the cell mortality induced by wild-type Aβ42 aggregates,[55] our current study demonstrates the high potency of Aβ42$_{DM}$ in inhibiting the cell toxicity that is mediated by a combination of PHF6 and Aβ42.

https://doi.org/10.1021/acschemneuro.1c00045
ACS Chem. Neurosci. 2021, 12, 1563−1577

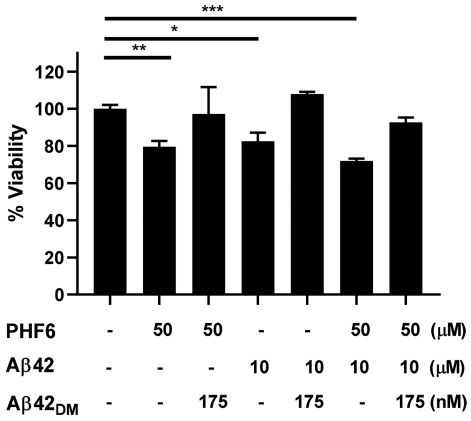

Figure 6. Aβ42$_{DM}$ inhibits toxicity mediated by both PHF6 and Aβ42. SH-SY5Y cells treated with synthetic PHF6, Aβ42, Aβ42$_{DM}$, or combinations of these peptides were incubated for 48 h, and cell viability was followed using XTT assay. Statistical analysis (n = 3) was performed with Student's t test: *, $P < 0.05$; **, $P < 0.01$; ***, $P < 0.005$; error bars indicate the standard error.

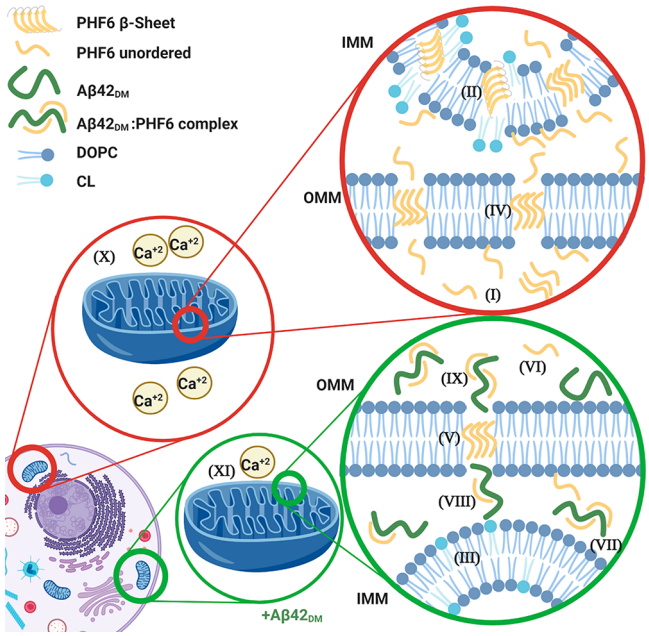

Figure 7. Scheme of Aβ42$_{DM}$ inhibition of PHF6-induced mitochondrial membrane damage. The red circles show the PHF6-induced disruption of the IMM in the absence of Aβ42$_{DM}$. In this process, PHF6 first interacts with the OMM and penetrates it without changing the fluidity of that membrane. Upon reaching the IMM, PHF6 adopts a predominantly β-sheet structure, and its interaction with the IMM reduces the fluidity of that membrane. The process of IMM disruption results in mitochondrial dysfunction, enhancement of intracellular calcium levels, and neuronal cell death. The green circles show the formation of a PHF6−Aβ42$_{DM}$ complex, which blocks the ability of PHF6 to disrupt the IMM. In this complex, PHF6 does not adopt the predominantly β-sheet structure needed to disrupt the IMM (through a reduction in membrane fluidity). Similarly, the complexed PHF6 does not form the predominantly β-sheet structure in the OMM that allows PHF6 to penetrate the OMM to reach the IMM. Thus, in the presence of Aβ42$_{DM}$, PHF6 does not change the fluidity of either the OMM or the IMM. This protective effect of Aβ42$_{DM}$ therefore interferes with the chain of mitochondrial dysfunction, enhancement of intracellular calcium levels, and neuronal cell death.

In light of our findings obtained with intact cells and with isolated and artificial membranes, we present a comprehensive, step-by-step mechanistic explanation for the protective effect of Aβ42$_{DM}$ against PHF6 toxicity, as demonstrated in Figure 7.

When in solution, as shown here and in previous studies,[43,52,66] PHF6 adopts a mixture of α-helix and β-sheet conformations (Figure 7, I), with nonaggregated PHF6 being predominantly helical[73,74] and aggregated PHF6 forming a densely packed, long, and uniform fibril conformation. In the presence of Aβ42$_{DM}$, an Aβ42 variant with a perturbed F19-L34 contact and reduced oligomerization, the secondary structure of PHF6 is abolished and fibril density decreases. In CL/DOPC (IMM model), but not in DOPC (OMM model), PHF6 undergoes a change in conformation to a predominantly β-sheet structure and hence forms densely packed uniform fibrils (Figure 7, II). In CL/DOPC, Aβ42$_{DM}$ prevents the formation of the β-sheet structure, and hence the PHF6 fibril density is reduced and the peptide is prevented from becoming embedded in CL/DOPC (Figure 7, III). Although there was an interaction between PHF6 and both DOPC (OMM) and CL/DOPC (IMM) phospholipids, in the DOPC samples in our study the less densely packed intact PHF6 fibrils were not embedded in the vesicles (Figure 7, IV) to the same extent as in the CL/DOPC vesicles (Figure 7, II). The small portion of PHF6 that was embedded in the OMM (Figure 7, IV and V), in the presence or absence of Aβ42$_{DM}$, was derived from unbound (not inhibited by Aβ42$_{DM}$) PHF6 (Figure 7, VI). Indeed, our ThT results showed that Aβ42$_{DM}$ has a much weaker inhibitory effect on PHF6 when the latter has low β-sheet content, as is the case in solution or in OMM environments (vs in the IMM).

In other words, we posit that to reach the IMM, PHF6 adopts a self-assembled compact structure to cross the OMM (Figure 7, IV and V) in an amyloid pore-formation-like mode of action.[19,75,76] This predominantly β-sheet structure (Figure S3C) causes much less disruption to the OMM and plasma membrane (as seen in both our TEM and anisotropy experiments with DOPC lipids) than to the IMM (DOPC/CL lipids), where it forms fibrils that affect membrane fluidity and the organization of the phospholipids. In solution and after interaction with the OMM, some fraction of PHF6 remains unbound, in both the presence and absence of Aβ42$_{DM}$. For example, in solution, a binding constant (K_d) of 1.03 ± 0.82 μM was determined for the Aβ42$_{DM}$−PHF6 complex, a value that is relatively low and is in keeping with the values for complexes of PHF6 with other known inhibitors.[21,55] The ability of the PHF6 fraction that is not bound to Aβ42$_{DM}$ to cross the OMM results from the apparent inability of Aβ42$_{DM}$ to complex the PHF6 in the form that it adopts when interacting with and permeating the OMM. With regard to the PHF6 that is bound to Aβ42$_{DM}$ (Figure 7, IX and VIII), our ITC experiments showed that the Aβ42$_{DM}$−PHF6 complex is stabilized mainly by hydrophobic interactions (as opposed to hydrogen bonding and electrostatic interactions), as this complex is characterized by entropy-favored interactions,[21,77,78] in accordance with the hydrophobic theory previously used to model protein folding to form fibrils.[79,80] This Aβ42$_{DM}$−PHF6 complex, in which PHF6 has adopted a nonfibrillar conformation, can neither permeate nor disrupt the IMM (Figure 7, VII). Our results showing Aβ42$_{DM}$ binding to PHF6 *in vitro* and to full-length tau in cells correlate with other studies that have characterized the interactions of Aβ42 and tau-MT-binding motifs.[81] These studies show that the R3

https://doi.org/10.1021/acschemneuro.1c00045
ACS Chem. Neurosci. 2021, 12, 1563−1577

motif that contains PHF6 undergoes both electrostatic and hydrophobic interactions with Aβ42, with the latter being more prevalent.

The stoichiometric binding ratio of n = 0.763 between Aβ42$_{DM}$ and PHF6 indicates that a single Aβ42$_{DM}$ molecule interacts with ~2 monomers of PHF6 (Figure 7, VII), which suggests binding of Aβ42$_{DM}$ to PHF6 at a very early stage of PHF6 oligomerization, thereby interfering with PHF6 fibrillation. This early stage inhibition, which is typical of other amyloid inhibitors, such as flavanols[82] and morin,[83] is crucial for inhibiting the formation of the oligomers that are considered to be the toxic species.[11,16]

As mentioned above, in addition to preventing PHF6 self-association, Aβ42$_{DM}$ also interferes with PHF6 binding to IMM phospholipids (Figure 7, VIII) but not to OMM phospholipids (Figure 7, V and IX). This is evident from our experiment with DPH-labeled artificial IMM, in which PHF6 binding to the lipids reduced bilayer fluidity (Figure 7, II). This effect was abolished upon treatment with Aβ42$_{DM}$ (Figure 7, III). In addition, PHF6 had no such effect on the fluidity of DPH-labeled artificial OMM (Figure 7, IV) or DOPC/DOPG (at 80:20 molar ratio) vesicles, also suggesting that while the presence of CL (a significant component of the IMM[39,71]) is obligatory for lipid interaction with PHF6, the presence of negatively charged lipids, such as DOPG, is not a criterion for binding. Although amyloids usually have an inherent preference for binding and interacting with anionic phospholipids,[40,62] our finding that PHF6 selectively binds CL in preference to the anionic DOPG is in line with a recent study showing that CL is essential for tau-mediated mitochondrial dysfunction.[42] Similarly, tau and tau-derived peptides with a single modification (Ac-PHF6 and NH_2-PHF6) were also shown to accumulate on an anionic DMPG [1,2-dimyristoyl-*sn*-glycero-3-phospho-(1′-rac-glycerol)] membrane monolayer surface[44] and to form β-sheet-rich structures that permeate those membranes, suggesting an important role for the anionic nature of the phospholipids in their interaction with these peptides.[40] We used a different PHF6 modification, namely, Ac-PHF6-NH_2, which may be the reason for the discrepancy between the above results and ours regarding the superior potency of the PHF6 that we used.

Other evidence for the preferential interaction of PHF6 with the IMM over the OMM and the ability of Aβ42$_{DM}$ to interfere with these interactions is given by our experiments in which COX activity and ζ-potential were measured. COX is located on the IMM, and its proper function is crucial for the mitochondrial respiratory system.[57] Our results with SMPs showed that PHF6 causes a dose−response reduction in COX activity, whereas a 1:286 (molar ratio) mixture of Aβ42$_{DM}$ and PHF6 abolished PHF6-induced reduction of COX activity. The finding that PHF6 disrupts the activity of COX, which is located on the IMM (and not on the OMM), complements indications from our other experiments as to the selective disrupting activity of PHF6 on the IMM vs the OMM and the finding that Aβ42$_{DM}$ could prevent IMM disruption. In a similar way, our results show that PHF6 caused an elevation in the ζ-potential of inverted but not noninverted SMPs, in a dose−response manner. Here again, when incubated at a molar ratio of 1:286 (Aβ42$_{DM}$:PHF6), Aβ42$_{DM}$ abolished the PHF6-mediated elevation of ζ-potential in inverted SMPs representing the IMM. These IMM disrupting activities, in turn, led to enhanced intracellular calcium levels in a dose-dependent manner (Figure 7, X). Once again, our experiments showed that in a cell culture treated with PHF6 together with Aβ42$_{DM}$ (at a molar ratio of 286:1), the PHF6-mediated intracellular calcium level elevation remained at levels similar to control levels (Figure 7, XI). In addition, our findings that PHF6, being a tau-derived peptide, caused an elevation in intracellular calcium levels (Figure 7, X) corroborates previous studies showing that tau induces an elevation of intracellular calcium levels.[17,36] When Aβ42$_{DM}$ was added to our system, this effect was suppressed (Figure 7, XI). A similar effect was also reported for the reversal by Aβ42$_{DM}$ of Aβ42-mediated intracellular calcium level elevation.[38]

In addition to the protective effect of Aβ42$_{DM}$ on PHF6−membrane interactions, Aβ42$_{DM}$ also facilitated a reduction in both cellular and mitochondrial tau accumulation. This result is in keeping with the findings of other studies that have shown a correlation between PHF6 and tau accumulation in cells and a reduction in cell viability[17,84] and an increase in mitochondrial dysfunction.[85,86] This reduction in tau levels may be due to an enhanced clearance that is mediated by Aβ42$_{DM}$ under the control of the ubiquitin−proteasome system[87] and/or autophagy,[88] both of which have been shown to be disrupted in AD.[89] For example, Aβ42$_{DM}$ may modulate tau levels in a similar way to that recently observed for Aβ40, which was shown to interfere with the cellular clearance pathway through hydrophobic interactions with ubiquitin.[90]

On the basis of the findings of this study and those of our previous studies,[38,55] we posit that Aβ42$_{DM}$ acts against both Aβ42 and tau via a similar protective mechanism. This mechanism is derived from the ability of Aβ42$_{DM}$ to (i) inhibit PHF6 from forming the predominately β-sheet structure that is required for interaction with both the OMM and the IMM but with selective disruption only of the IMM, (ii) interact with both Aβ42 and PHF6 and thereby to modify their amyloid-forming pathway by reducing their ability to permeate the OMM and reach the IMM and hence their ability to disrupt the IMM and cause mitochondrial dysfunction, and (iii) form a Aβ42$_{DM}$:tau complex with reduced cell toxicity, a complex that, unlike its separate components, does not tend to accumulate in cells.

MATERIALS AND METHODS

Reagents and Cells. The peptide Aβ(1−42) with two mutations F19S and L34P, designated Aβ42$_{DM}$, and Ac-PHF6-NH_2 (designated synthetic PHF6) were chemically synthesized and purchased from GL-Biochem (Shanghai, China). The SH-SY5Y neuroblastoma cell line was grown at 37 °C and 5% CO_2 in Dulbecco's modified Eagle medium (DMEM) supplemented with 10% tetracycline-free fetal bovine serum, L-glutamine (2 mM), and penicillin (100 units/mL)/streptomycin (0.1 mg/mL) (Gibco, Israel). Transfection of SH-SY5Y cells was performed using the jetOPTIMUS transfection reagent (Tamar, Israel) according to the manufacturer's protocol. Empty plasmids were transfected and used as control. The plasmids, pRRL tau$_{K174Q}$ and mEmerald-MAP-tau$_{K174Q}$-N-10-Flag (Addgene, MA, USA) (Em-Tau), ApoAlert, and pHAGE Aβ42$_{F19S,L34P}$-GFP (Aβ42$_{DM}$-GFP), Phage Aβ42$_{DM}$ and pHAGE empty plasmids were generated in our lab.[55] 1,2-Dioleoyl-*sn*-glycero-3-phosphocholine (DOPC), cardiolipin (bovine heart) sodium salt (CL), and 1,2-dioleoyl-*sn*-glycero-3-phospho-(1′-rac-glycerol) sodium salt (DOPG) were purchased from Avanti Polar Lipids (AL, USA).

Primary Cortical Culture. Plugged female mice were killed, and embryos were harvested between days E13.5 and E15. Brains were dissected out, and cortices were removed and collected into Hanks' balanced salt solution (HBSS) buffer. Cortices were then stripped of the meninges, minced, and dissociated in HBSS buffer with papain for

https://doi.org/10.1021/acschemneuro.1c00045
ACS Chem. Neurosci. 2021, 12, 1563−1577

15 min. Tissues were washed and mechanically dissociated with glass pipettes. Cells were then plated at a density of 50 000 cells/well in 96-well plates coated with poly-L-lysine (0.05 mg/mL; P-4707; Sigma, St. Louis, MO) in neurobasal medium (Gibco), supplemented with B-27 (Gibco), GlutaMAX (Gibco), and 2% fetal bovine serum (HyClone). After 24 h, the medium was replaced with serum-free neurobasal medium, supplemented with B-27 and GlutaMAX. After 7 days, cells were infected with an adenovirus.

XTT Cell Viability and Cell Count Assays. The viability of SH-SY5Y cells transfected with tau_{K174Q} in the absence or presence of different quantities of $A\beta42_{DM}$ (i.e., 0.5 μg of tau_{K174Q} with 0.25 μg, 0.5 μg, or 1 μg of $A\beta42_{DM}$) or alternatively treated with extracellular PHF6 (50 μM), $A\beta42_{DM}$ (175 nM) or a combination of the two (i.e., 50 μM of PHF6 with 64 nM, 175 nM, or 500 nM $A\beta42_{DM}$) was assessed using an XTT-based kit (Biological Industries, CT, USA). The viability of SH-SY5Y cells incubated with both PHF6 (50 μM) and Aβ42 (10 μM) and untreated or treated with $A\beta42_{DM}$ (175 nM) was performed in a similar way. Briefly, $\sim 1 \times 10^4$ cells per well were seeded in a 96-well tissue culture plate (Costar, Sigma-Aldrich, Israel) and incubated at 37 °C in a 5% CO_2 atmosphere. Forty-eight hours after treatments were performed (transfection with DNA and addition of the peptides), 30 μL of XTT reagent was added to each well, and the plate was read at 465 and 660 nm using a BioTek Synergy 4 microplate reader (Winooski, VT, USA). Untreated SH-SY5Y cells and cells transfected with empty plasmid served as controls. Data for each sample, performed in triplicate, are presented as percentage of control.

For primary cortical cells experiments, 5×10^4 cells were infected with adeno-associated virus 2 (AAV2) containing either FLAG-Emerald-tau_{K174Q} or $A\beta42_{DM}$ genes, both serving as controls. For test samples, 3 days postinfection with FLAG-Emerald-tau_{K174Q} gene, the cells were co-infected with $A\beta42_{DM}$ gene. After 8 days from the first infection (in both control and test samples), 20 μL of XTT reagent was added to each well, and the plate was read at 465 and 660 nm using a BioTek Synergy 4 microplate reader (Winooski, VT, USA). The live cell count was obtained by using Countess II automated cell counter (Thermo Fisher, Israel). The experimental procedure and analysis were the same as for the XTT assay except that 48 h after treatment, each sample was incubated with trypsin for 5 min, neutralized with DMEM, centrifuged for 5 min, and resuspended in 1 mL of DMEM. Each cell mixture (10 μL) was mixed with 10 μL of trypan blue and pipetted into a Countess chamber slide for sample count and analysis.

Crystal Violet Staining of Living Cells in Primary Culture. For crystal violet solution, 0.125 g of crystal violet (Sigma-Aldrich, Israel) was diluted in 50 mL of 20% methanol. After 48 h incubation of the primary cells with different treatments (500 nM $A\beta42_{DM}$, 5 μM PHF6, or a mixture of 5 μM PHF6 and 64 nM $A\beta42_{DM}$), the supernatants were removed, and the plates were washed gently three times with doubly distilled water. Subsequently, 100 μL of crystal violet solution was added to each well. After 30 min of staining, the excess crystal violet was washed off with doubly distilled water. Finally, the fixed crystal violet was released by the addition of 100 μL of 2% SDS solution to each well, and the plates were read at 550 nm with a BioTek Synergy 4 microplate reader.

Tau Accumulation in Cells. To follow tau_{K174Q} accumulation in whole cells, SH-SY5Y cells were grown on six-well plates (1×10^5 cells per well). The cells were transfected to express Flag-tau_{K174Q}-GFP, $A\beta42_{DM}$, or a combination of the two (at 2:1, 1:1, and 1:2 Flag-tau_{K174Q}-GFP:$A\beta42_{DM}$ DNA ratio) using a total of 2 μg of DNA. After 48 h, the cells were harvested and washed with PBS. The cell pellet was then suspended in RIPA buffer (25 mM HEPES−NaOH, 150 mM KCl, 1 mM EDTA, 1% Triton X-100, 0.1% NP-40, pH 7.4) and a freshly prepared cocktail of protease inhibitors (PI) (1:200; Sigma−Aldrich, Israel) and then sonicated. Protein concentrations were determined by Bradford assay (Bio-Rad, Hercules, CA). Total cell lysates (100 μg) were supplemented with sample buffer and loaded on 12.5% SDS−PAGE. Following transfer to nitrocellulose membranes, distinct protein bands were identified with anti-Flag (Sigma-Aldrich, Israel) or anti-β tubulin antibodies (Abcam, Cambridge, U.K.). HRP-conjugated anti-mouse and anti-rabbit antibodies (Jackson, PA, USA) were used as secondary antibodies for analysis. Antibody labeling was identified by using an enhanced chemiluminescence kit (Biological Industries, IL).

Tau Accumulation in the Mitochondria. To follow tau_{K174Q} accumulation in the mitochondria in the absence or presence of $A\beta42_{DM}$, 4×10^6 naïve SH-SY5Y cells were seeded in 10 cm plates. The cells were transfected to express Flag-tau_{K174Q}-GFP alone or in combination with $A\beta42_{DM}$ (at 1:1 Flag-tau_{K174Q}-GFP:$A\beta42_{DM}$ ratio) using a total of 2 μg of DNA. The cells (1×10^7) were harvested at 75−80% confluence. The cell pellet was rinsed with 5 mL of hypotonic solution (100 mM sucrose, 20 mM MOPS−KOH, pH 7.2) and precipitated by centrifugation at 800g for 5 min at 4 °C. The cell suspension was diluted with 750 μL of isolation buffer [100 mM sucrose, 20 mM MOPS−KOH, pH 7.2, 5% Percoll, 150 μM PMSF, 5 μg/mL leupeptin, 1:1000 fresh PI cocktail (1:200; Sigma-Aldrich, Israel)] per sample and incubated on ice for 5 min. The swollen cells were broken with several (15) strokes in a homogenizer (0.5 mL of isolation buffer) on ice and precipitated by centrifugation at 2500g for 5 min at 4 °C. The precipitation step was repeated twice. The supernatants were pooled and precipitated by centrifugation at 10 000g for 10 min at 4 °C. The final pellet was resuspended in 100 μL of working solution (220 mM mannitol, 70 mM sucrose, 20 mM MOPS−KOH, pH 7.2) and stored at −80 °C until used.

For measuring the level of tau in the mitochondria, the following procedure was used: The mitochondria isolated from each sample (transfected tau_{K174Q} alone, transfected tau_{K174Q} and $A\beta42_{DM}$, and untransfected SH-SY5Y control cells) were supplemented with sample buffer, boiled, and separated on a 15% SDS−PAGE gel. Western-blot analysis was performed using anti-Flag (Sigma-Aldrich, Israel) for Flag-tau_{K174Q}-GFP detection and anti-VDAC1 (Abcam, Cambridge, U.K.) for VDAC1 detection, as VDAC1 is a mitochondrial housekeeping gene.[91] Secondary antibodies were used as mentioned above for the analysis.

Immunoprecipitation Experiments. To detect the interaction of $A\beta42_{DM}$ with tau_{K174Q} in cells, 4×10^6 naïve SH-SY5Y cells were seeded in 10 cm plates. The cells were transfected to express tau_{K174Q}, $A\beta42_{DM}$-GFP, or both by using a total of 10 μg of DNA. The cells were harvested and lysed using an immunoprecipitation (IP) buffer [20 mM Tris-HCl, pH 7.6, 200 mM NaCl, 0.72 mM EDTA, 10% glycerol, 7 mM DTT, PI cocktail (Sigma-Aldrich, Israel), which was added fresh before use at a ratio of 1:200, and 0.15% Triton X-100]. The solubilized cell fraction was incubated with magnetic protein G Dynabeads (Bio-Rad, Hercules, CA) according to the manufacturer's instructions. The beads were magnetically isolated and washed three times with PBS, incubated with rabbit anti-GFP antibody (Abcam, Cambridge, MA), and suspended in sample buffer [50 mM Tris-HCl, pH 7.5, 0.5 M KCl, 1% NP40, 0.5 mM 1,4-dithiothreitol (DTT), 0.2 mM PMSF, and phosphatase inhibitor (ApexBio, Houston, TX)]. The samples were heated for 5 min at 95 °C, separated by 10% SDS−PAGE, and subjected to Western blot analysis. Proteins in the gel were transferred to a nitrocellulose membrane, which was probed with mouse anti-Aβ42 IgG antibody (Sigma-Aldrich, Huston, TA) diluted 1/1000 in PBS to detect $A\beta42_{DM}$-GFP fusion protein or with mouse anti-tau-1 antibody (Sigma-Aldrich, Huston, TA) diluted 1/1000 in PBS to detect tau_{K174Q}. HRP-conjugated anti-mouse and anti-rabbit antibodies (Jackson, PA, USA) were used as secondary antibodies. Antibody binding was monitored using an enhanced chemiluminescence kit (Biological Industries). Ponceau S (Cell Signaling Technology, Danvers, MA) was used to confirm equal loading of cell-expressed proteins in all samples.

Isothermal Titration Calorimetry (ITC). ITC was performed as described previously.[92] Fresh PHF6 and $A\beta42_{DM}$ were diluted to 400 μM and 50 μM, respectively, in 20 mM MOPS, pH 7.2. A sample of 350 μL of $A\beta42_{DM}$ was inserted into a Nano ITC low volume cell (TA Instruments, DE, USA), and the titrating syringe was loaded with 50 μL of PHF6 solution. The system was allowed to reach a stable temperature of 25 °C for 2000 s, followed by measurement of baseline signal for 500 s. Thereafter, 47.5 μL of the PHF6 solution was titrated dropwise into the $A\beta42_{DM}$ solution or into the MOPS blank (for

https://doi.org/10.1021/acschemneuro.1c00045
ACS Chem. Neurosci. 2021, 12, 1563−1577

baseline correction) in 5 μL aliquots (except for the first drop, whose volume, in practice, was 2.5 μL); each drop was allowed to equilibrate for 300 s before adding the next drop of PHF6 to Aβ42$_{DM}$. The resulting binding isotherm was analyzed by Nanoanalyze software using an independent interaction model.[21]

Formation of Submitochondrial Particles (SMPs). For preparation of SMPs, we isolated mitochondria from SH-SY5Y cells by using a previously described method.[38] Briefly, SH-SY5Y cells were harvested at 75−80% confluence. A mass of 1 g of the cell pellet was rinsed with 10 mL of hypotonic solution (100 mM sucrose, 10 mM MOPS, pH 7.2, 1 mM EGTA) to allow the cells to swell, followed by incubation of the cells for 10 min on ice; 2 mL portions of the suspension were then homogenized with a Teflon glass homogenizer with gentle circular strokes. The cell suspension was diluted with hypertonic solution (1.25 M sucrose, 10 mM MOPS, pH 7.2) in a ratio of 1 mL of hypertonic solution to 10 mL of cell suspension to restore solution isotonicity. The cell aliquots were then diluted with six volumes of isolation buffer [75 mM mannitol, 225 mM sucrose, 10 mM MOPS, pH 7.2, 1 mM EGTA, and 0.1% fatty acid free bovine serum albumin (BSA)]. Cellular detritus was precipitated by centrifugation at 2000 rpm for 5 min at 4 °C. The supernatant containing the mitochondria was then centrifuged at 14 000 rpm for 25 min at 4 °C. The resulting crude mitochondrial pellet was rinsed by centrifugation under the same conditions (14 000 rpm, 4 °C for 25 min) in 15 mL of MiR06 buffer (110 mM sucrose, 60 mM K-lactobionate, 20 mM HEPES, pH 7.2, 1 mM KH_2PO_4, 3 mM $MgCl_2 \cdot 6H_2O$, 0.5 mM EGTA, 20 mM taurine, and 0.1% fatty acid free BSA). The final pellet, containing the mitochondria, was resuspended in 100 μL of MiR06 by vortexing and stored at −80 °C until used.

Inverted SMPs were prepared according to a known protocol.[93] Before use, the suspensions of the mitochondria were diluted to 2 mL volumes with sonication buffer (250 mM sucrose, 1 mM EDTA, and 10 mM Tris-HCl, pH 7.2). The mitochondrial suspension was probe sonicated for 30 s on ice, using 20% amplitude and 5 s on/off sonication cycles, to form inside-out oriented SMPs (in which the IMM faced outward to the medium solution). The solution of SMPs was centrifuged at 8000 rpm to remove large remaining fragments of mitochondrial membranes. The concentration of SMPs (μg protein/mL) was determined by the Bradford assay. The inversion of the IMM in the SMPs was verified by a COX activity assay (see next section).

Cytochrome *c* Oxidase (COX) Activity. COX activity was determined by monitoring the decrease in absorbance at 550 nm of chemically reduced ferrocytochrome *c* solution in the presence of SMPs. The ferrocytochrome *c* substrate solution (0.22 mM) was prepared by addition of 0.1 M DTT to 2.7 mg/mL of COX dissolved in purified water and PI cocktail 1:200 (Sigma-Aldrich, Israel). Samples of SH-SY5Y SMPs (200 μg/mL final concentration) were mixed with increasing concentrations of PHF6 (10−200 μM), Aβ42$_{DM}$ (175 nM), or a combination of the two (i.e., 50 μM PHF6 with 175 nM Aβ42$_{DM}$), and each protein/SMP mixture sample was supplemented with 950 μL of assay buffer (10 mM Tris-HCl, 120 mM KCl, pH 7.0). Enzyme buffer (10 mM Tris-HCl, 250 mM sucrose, pH 7.0) was then added to bring the total reaction volume to 1.1 mL. To initiate the oxidation reaction between ferricytochrome *c* and COX, a 50 μL portion of ferrocytochrome *c* substrate solution was added to the protein/SMP mixture samples to start the reaction. Aliquots of 200 μL of each reaction sample were measured in 5 repeats in 96-well plates. The kinetic changes of absorbance were measured at 25 °C for 20 min, with 20 s intervals, on a BioTek Synergy 4 microplate reader (Winooski, VT, USA). The activity of COX (units/ml) was calculated according to eq 1.

$$\text{COX activity}\left(\frac{\text{units}}{\text{mL}}\right) = \frac{\Delta A/\text{sec} \times \text{dil} \times \text{V(t)}}{\text{V(s)} \times 21.84} \quad (1)$$

where ΔA/sec is the reaction rate of a sample subtracted from blank, dil is the dilution factor of ferrocytochrome *c* solution, V(t) is the total reaction volume, V(s) is the volume of ferrocytochrome *c* substrate added to initiate oxidation, and the value 21.84 is the extinction coefficient between ferrocytochrome *c* and ferricytochrome *c* at 550 nm.[94] The COX assay was performed according to the manufacturer's protocol (Sigma-Aldrich, Israel). Unit definition: One unit oxidizes 1.0 μmole of ferrocytochrome *c* per second at pH 7.0, 25 °C.

Determination of Intracellular Calcium. For measuring intracellular calcium levels, 1×10^4 SH-SY5Y cells per well were seeded in black clear-bottomed 96-well plates (Costar, Sigma-Aldrich, Israel). Cells were treated with PHF6 (10 μM or 50 μM in purified water) in the absence or presence of Aβ42$_{DM}$ (175 nM in purified water) for 48 h. The cells were subjected to an intracellular calcium assay using the Fluo-4 Direct calcium assay kit (Thermo-Fisher, Israel), according to the manufacturer's protocol, which facilitates measurement of the increase in fluorescence relative to a nontreated control as a result of increase in the intracellular calcium levels. Changes of fluorescence emission were measured by using a Synergy2 microplate spectrophotometer (BioTek, Winooski, VT) with fluorescence excitation and emission wavelengths of 494 and 516 nm, respectively.

ζ-Potential of Inverted and Noninverted SMPs. The ζ-potential of SMPs that were treated with increasing concentrations of PHF6 (5−100 μM), Aβ42$_{DM}$ (175 nM), and combination of the two (i.e., 50 μM PHF6 with 175 nM Aβ42$_{DM}$) was measured by Zetasizer (Zetasizer Nano ZS, Malvern, Worcestershire, U.K.), and data were subsequently analyzed using the Smoluchowski model, which is provided as part of the instrument analysis computational package. Noninverted SMPs used in this assay were prepared as described above except EDTA that was excluded from the sonication buffer (250 mM sucrose, 1 mM EDTA, and 10 mM Tris-HCl, pH 7.2).

Preparation of Small Unilamellar Vesicles (SUVs). Lipid constituents were dissolved in a chloroform/ethanol solution (1:1 molar ratio) and dried together under vacuum to constant weight, followed by addition of sodium phosphate buffer (pH 7.4) and probe-sonication for 10 min at room temperature, with 20% amplitude and on/off 59 s cycles. For all the experiments with SUVs, the final total concentration of lipids was 1 mM.

Thioflavin T (ThT) Fluorescence Assay. ThT fluorescence measurements to follow aggregation in reactions were conducted at 25 °C using 96-well path cell culture plates on a BioTek Synergy 4 microplate reader (Winooski, VT, USA). A 120 μL aliquot of the aggregation reaction mixture was mixed with 10 μM ThT in sodium phosphate buffer (pH 7.4). The fluorescence intensity was measured at λ_{ex} = 440 and λ_{em} = 485 nm and followed for 20−24 h. PHF6 (50 μM) in the presence or absence of Aβ42$_{DM}$ (175 nM) in sodium phosphate buffer (pH 7.4) was used in four samples, one with buffer only and the other three samples each with a different reagent, namely, heparin (10 μM), DOPC, and CL/DOPC (10:90) SUVs (0.4 mM).

Transmission Electron Microscopy (TEM). Sample aliquots (5 μL), similar to those that were used in the ThT experiment described above, were placed on 400-mesh copper grids covered with a carbon-stabilized Formvar film. Excess solution was removed following 2 min of incubation, and the grids were negatively stained for 30 s with a 1% uranyl acetate solution. Samples were viewed in a FEI Tecnai 12 TWIN TEM operating at 120 kV.

Circular Dichroism (CD) Measurements. Spectra were recorded on a Jasco J715 spectropolarimeter over a range of 185−260 nm using a quartz cuvette with a path length of 1 mm, a scanning speed of 50 nm/min, and a data interval of 0.5 nm, at 25 °C. PHF6 (50 μM) was allowed to react in the presence or absence of either Aβ42$_{DM}$ (175 nM), heparin (10 μM), CL/DOPC (10:90) SUVs, or buffer (0.15 M NaCl, 10 mM sodium phosphate, pH 7.4). Buffer alone served as the background. Each sample was scanned four times 24 h post incubation.

Fluorescence Anisotropy. As previously described,[95−97] the fluorescent probe DPH was incorporated into DOPC, DOPC/CL (90:10), and DOPC/DOPG (80:20) SUVs. Briefly, DPH was dissolved in tetrahydrofuran (1 mg/mL) and the solution was added to 1 mM vesicles in a molar ratio of 1:400 (probe:SUVs). After 30 min of incubation at 25 °C with DPH, the vesicles supplemented with fluorescent dye were mixed with different concentrations of the

https://doi.org/10.1021/acschemneuro.1c00045
ACS Chem. Neurosci. 2021, 12, 1563−1577

following peptides: PHF6 (10−400 μM), Aβ42$_{DM}$ (175 nM), and a mixture of either 50 or 400 μM PHF6 with Aβ42$_{DM}$ (175 nM). Fluorescence anisotropy was performed at λ_{ex} = 360 nm and λ_{em} = 430 nm using a FL920 spectrofluorometer (Edinburgh Co., Edinburgh, U.K.). Data were collected prior to and following addition of freshly dissolved PHF6 and Aβ42$_{DM}$. Anisotropy values were automatically calculated by the spectrofluorometer software using eq 2,

$$r = (I_{VV} - GI_{VH})/(I_{VV} + 2GI_{VH}), \quad G = I_{VH}/I_{HH} \tag{2}$$

where I_{VV} corresponds to the excitation and emission polarizers mounted vertically; I_{HH}, to the excitation and emission polarizers mounted horizontally; I_{HV}, to the excitation polarizer in the horizontal position and the emission polarizer in the vertical position; and I_{VH}, to the excitation polarizer vertical and emission polarizer horizontal.

Statistical Analyses. Unless otherwise indicated, each experiment was performed in triplicate and the results are mean values ± SEM. Statistical significance was determined using ordinary one-way ANOVA test.

■ ASSOCIATED CONTENT

Supporting Information

The Supporting Information is available free of charge at https://pubs.acs.org/doi/10.1021/acschemneuro.1c00045.

A scheme describing tau and derived fragments, cytochrome *c* oxidase activity in submitochondrial particles (SMPs), and a ThT activity graph and TEM image of PHF6 in DOPC vesicles (PDF)

■ AUTHOR INFORMATION

Corresponding Author

Niv Papo − *Avram and Stella Goldstein-Goren Department of Biotechnology Engineering and the National Institute of Biotechnology in the Negev, Ben-Gurion University of the Negev, Beer-Sheva 84105, Israel;* orcid.org/0000-0002-7056-2418; Phone: +972-50-2029729; Email: papo@bgu.ac.il

Authors

Segev Naveh Tassa − *Avram and Stella Goldstein-Goren Department of Biotechnology Engineering and the National Institute of Biotechnology in the Negev, Ben-Gurion University of the Negev, Beer-Sheva 84105, Israel*

Shani Ben Zichri − *Department of Chemistry, Ben-Gurion University of the Negev, Beer-Sheva 84105, Israel*

Shiran Lacham-Hartman − *Avram and Stella Goldstein-Goren Department of Biotechnology Engineering and the National Institute of Biotechnology in the Negev, Ben-Gurion University of the Negev, Beer-Sheva 84105, Israel*

Ofek Oren − *The Shraga Segal Department of Microbiology, Immunology and Genetics, Faculty of Health Sciences, Ben-Gurion University of the Negev, Beer-Sheva 84105, Israel*

Zeev Slobodnik − *Department of Life Sciences, Ben-Gurion University of the Negev, Beer-Sheva 84105, Israel; The Zlotowski Center for Neuroscience, Ben-Gurion University of the Negev, Beer Sheva 84105, Israel*

Ekaterina Eremenko − *Department of Life Sciences, Ben-Gurion University of the Negev, Beer-Sheva 84105, Israel; The Zlotowski Center for Neuroscience, Ben-Gurion University of the Negev, Beer Sheva 84105, Israel*

Debra Toiber − *Department of Life Sciences, Ben-Gurion University of the Negev, Beer-Sheva 84105, Israel; The Zlotowski Center for Neuroscience, Ben-Gurion University of the Negev, Beer Sheva 84105, Israel*

Raz Jelinek − *Department of Chemistry, Ben-Gurion University of the Negev, Beer-Sheva 84105, Israel;* orcid.org/0000-0002-0336-1384

Complete contact information is available at: https://pubs.acs.org/10.1021/acschemneuro.1c00045

Author Contributions

S.N.T., S.B.Z., and N.P. designed the research. S.N.T., S.B.Z, S.L.-H., Z.S., and E.E. performed the research. S.N.T., S.B.Z., O.O., Z.S., D.T., R.J., and N.P. analyzed the data. S.N.T. and N.P. wrote the paper. All authors edited the manuscript and approved the final version.

Notes

The authors declare no competing financial interest.

■ ACKNOWLEDGMENTS

The authors thank Dr. Sofiya Kulosheva for the technical assistance. This work was supported by the European Research Council "Ideas Program" ERC-2013-StG (Contract Grant 336041) and the Israel Science Foundation (Grant 615/14) to N.P. and grants from the David and Inez Myers Foundation and the Israel Ministry of Science & Technology (Contract Grant 100550) to D.T.

■ ABBREVIATIONS USED

Aβ, amyloid β; Aβ42, amyloid β 1−42; Aβ42$_{DM}$, amyloid β 1−42 double mutant; AD, Alzheimer's disease; APP, amyloid precursor protein; BSA, bovine serum albumin; CD, circular dichroism; CL, cardiolipin; COX, cytochrome *c* oxidase; DMEM, Dulbecco's modified Eagle's medium; DOPC, 1,2-dioleoyl-*sn*-glycero-3-phosphocholine; DOPG, 1,2-dioleoyl-*sn*-glycero-3-phospho-(1′-rac-glycerol); DPH, 1,6-diphenyl-1,3,5-hexatriene; IMM, inner mitochondrial membrane; LUV, large unilamellar vesicle; NFT, neurofibrillary tangle; OMM, outer mitochondrial membrane; PBS, phosphate buffered saline; PHF, paired helical filament; SF, straight filament; SMP, submitochondrial particle; SUV, small unilamellar vesicle

■ REFERENCES

(1) Alzheimer's Disease International, McGill University. (September 21, 2020) *World Alzheimer Report 2020.*

(2) Nussbaum, J. M., Seward, M. E., and Bloom, G. S. (2013) Alzheimer Disease: A Tale of Two Prions. *Prion 7* (1), 14−19.

(3) Selkoe, D. J. (2003) Folding Proteins in Fatal Ways. *Nature 426*, 900−904.

(4) Lin, M. T., and Beal, M. F. (2006) Alzheimer's APP Mangles Mitochondria. *Nat. Med. 12*, 1241−1243.

(5) Drolle, E., Hane, F., Lee, B., and Leonenko, Z. (2014) Atomic Force Microscopy to Study Molecular Mechanisms of Amyloid Fibril Formation and Toxicity in Alzheimer's Disease. *Drug Metab. Rev. 46*, 207−223.

(6) Demuro, A., Mina, E., Kayed, R., Milton, S. C., Parker, I., and Glabe, C. G. (2005) Calcium Dysregulation and Membrane Disruption as a Ubiquitous Neurotoxic Mechanism of Soluble Amyloid Oligomers. *J. Biol. Chem. 280* (17), 17294−17300.

(7) Morita, M., Vestergaard, M., Hamada, T., and Takagi, M. (2010) Real-Time Observation of Model Membrane Dynamics Induced by Alzheimer's Amyloid Beta. *Biophys. Chem. 147* (1−2), 81−86.

(8) Zempel, H., Thies, E., Mandelkow, E., and Mandelkow, E.-M. (2010) A Oligomers Cause Localized Ca2+ Elevation, Missorting of Endogenous Tau into Dendrites, Tau Phosphorylation, and Destruction of Microtubules and Spines. *J. Neurosci. 30* (36), 11938−11950.

(9) Pagani, L., and Eckert, A. (2011) Amyloid-Beta Interaction with Mitochondria. *Int. J. Alzheimer's Dis. 2011*, 925050.
(10) Kashyap, G., Bapat, D., Das, D., Gowaikar, R., Amritkar, R. E., Rangarajan, G., Ravindranath, V., and Ambika, G. (2019) Synapse Loss and Progress of Alzheimer's Disease -A Network Model. *Sci. Rep. 9*, 6555.
(11) Lee, S. J. C., Nam, E., Lee, H. J., Savelieff, M. G., and Lim, M. H. (2017) Towards an Understanding of Amyloid-β Oligomers: Characterization, Toxicity Mechanisms, and Inhibitors. *Chem. Soc. Rev. 46*, 310−323.
(12) Dehmelt, L., and Halpain, S. (2004) The MAP2/Tau Family of Microtubule-Associated Proteins. *Genome Biology. 6*, 204.
(13) Šimić, G., Babić Leko, M., Wray, S., Harrington, C., Delalle, I., Jovanov-Milošević, N., Bažadona, D., Buée, L., de Silva, R., Di Giovanni, G., Wischik, C., and Hof, P. R. (2016) Tau Protein Hyperphosphorylation and Aggregation in Alzheimer's Disease and Other Tauopathies, and Possible Neuroprotective Strategies. *Biomolecules 6*, 6.
(14) Min, S.-W., Chen, X., Tracy, T. E., Li, Y., Zhou, Y., Wang, C., Shirakawa, K., Minami, S. S., Defensor, E., Mok, S. A., Sohn, P. D., Schilling, B., Cong, X., Ellerby, L., Gibson, B. W., Johnson, J., Krogan, N., Shamloo, M., Gestwicki, J., Masliah, E., Verdin, E., and Gan, L. (2015) Critical Role of Acetylation in Tau-Mediated Neurodegeneration and Cognitive Deficits. *Nat. Med. 21*, 1154.
(15) Crowther, R. A. (1991) Straight and Paired Helical Filaments in Alzheimer Disease Have a Common Structural Unit. *Proc. Natl. Acad. Sci. U. S. A. 88* (6), 2288−2292.
(16) Meraz-Ríos, M. A., Lira-De León, K. I., Campos-Peña, V., De Anda-Hernández, M. A., and Mena-López, R. (2010) Tau Oligomers and Aggregation in Alzheimer's Disease. *J. Neurochem. 112* (6), 1353−1367.
(17) Moreno, H., Morfini, G., Buitrago, L., Ujlaki, G., Choi, S., Yu, E., Moreira, J. E., Avila, J., Brady, S. T., Pant, H., Sugimori, M., and Llinás, R. R. (2016) Tau Pathology-Mediated Presynaptic Dysfunction. *Neuroscience 325* (March), 30−38.
(18) Fitzpatrick, A. W. P., Falcon, B., He, S., Murzin, A. G., Murshudov, G., Garringer, H. J., Crowther, R. A., Ghetti, B., Goedert, M., and Scheres, S. H. W. (2017) Cryo-EM Structures of Tau Filaments from Alzheimer's Disease. *Nature 547* (7662), 185−190.
(19) Serra-Batiste, M., Ninot-Pedrosa, M., Bayoumi, M., Gairí, M., Maglia, G., and Carulla, N. (2016) Aβ42 Assembles into Specific β-Barrel Pore-Forming Oligomers in Membrane-Mimicking Environments. *Proc. Natl. Acad. Sci. U. S. A. 113* (39), 10866−10871.
(20) Lasagna-Reeves, C. A., Sengupta, U., Castillo-Carranza, D., Gerson, J. E., Guerrero-Munoz, M., Troncoso, J. C., Jackson, G. R., and Kayed, R. (2014) The Formation of Tau Pore-like Structures Is Prevalent and Cell Specific: Possible Implications for the Disease Phenotypes. *Acta Neuropathol. Commun. 2*, 56.
(21) Viswanathan, G. K., Shwartz, D., Losev, Y., Arad, E., Shemesh, C., Pichinuk, E., Engel, H., Raveh, A., Jelinek, R., Cooper, I., Gosselet, F., Gazit, E., and Segal, D. (2020) Purpurin Modulates Tau-Derived VQIVYK Fibrillization and Ameliorates Alzheimer's Disease-like Symptoms in Animal Model. *Cell. Mol. Life Sci. 77* (14), 2795−2813.
(22) Murugan, N. A., Nordberg, A., and Ågren, H. (2018) Different Positron Emission Tomography Tau Tracers Bind to Multiple Binding Sites on the Tau Fibril: Insight from Computational Modeling. *ACS Chem. Neurosci. 9* (7), 1757−1767.
(23) Mangialasche, F., Solomon, A., Winblad, B., Mecocci, P., and Kivipelto, M. (2010) Alzheimer's Disease: Clinical Trials and Drug Development. *Lancet Neurol. 9* (7), 702−716.
(24) Aisen, P. S., Gauthier, S., Ferris, S. H., Saumier, D., Haine, D., Garceau, D., Duong, A., Suhy, J., Oh, J., Lau, W. C., and Sampalis, J. (2011) Tramiprosate in Mild-to-Moderate Alzheimer's Disease - A Randomized, Double-Blind, Placebo-Controlled, Multi-Centre Study (the Alphase Study). *Arch. Med. Sci. 1*, 102−111.
(25) Tariot, P. N., and Aisen, P. S. (2009) Can Lithium or Valproate Untie Tangles in Alzheimer's Disease? *J. Clin. Psychiatry 70*, 919−921.
(26) Ivashko-Pachima, Y., Maor-Nof, M., and Gozes, I. (2019) NAP (Davunetide) Preferential Interaction with Dynamic 3-Repeat Tau Explains Differential Protection in Selected Tauopathies. *PLoS One 14* (3), No. e0213666.
(27) Shiryaev, N., Jouroukhin, Y., Giladi, E., Polyzoidou, E., Grigoriadis, N. C., Rosenmann, H., and Gozes, I. (2009) NAP Protects Memory, Increases Soluble Tau and Reduces Tau Hyperphosphorylation in a Tauopathy Model. *Neurobiol. Dis. 34* (2), 381−388.
(28) Guo, J. P., Arai, T., Miklossy, J., and McGeer, P. L. (2006) Aβ and Tau Form Soluble Complexes That May Promote Self Aggregation of Both into the Insoluble Forms in Alzheimer's Diseases. *Proc. Natl. Acad. Sci. U. S. A. 103* (6), 1953−1958.
(29) Ittner, L. M., and Götz, J. (2011) Amyloid-β and Tau - A Toxic Pas de Deux in Alzheimer's Disease. *Nat. Rev. Neurosci. 12* (2), 67−72.
(30) Gotz, J., and Chen, J. (2001) Formation of Neurofibrillary Tangles in P301l Tau Transgenic Mice Induced by Aβ42 Fibrils. *Science 293*, 1491−1495.
(31) Jacobs, H. I. L., Hedden, T., Schultz, A. P., Sepulcre, J., Perea, R. D., Amariglio, R. E., Papp, K. V., Rentz, D. M., Sperling, R. A., and Johnson, K. A. (2018) Structural Tract Alterations Predict Downstream Tau Accumulation in Amyloid-Positive Older Individuals. *Nat. Neurosci. 21* (3), 424−431.
(32) Jagust, W. (2018) Imaging the Evolution and Pathophysiology of Alzheimer Disease. *Nat. Rev. Neurosci. 19*, 687−700.
(33) Vossel, K. A., Zhang, K., Brodbeck, J., Daub, A. C., Sharma, P., Finkbeiner, S., Cui, B., and Mucke, L. (2010) Tau Reduction Prevents Aβ-Induced Defects in Axonal Transport. *Science 330*, 198.
(34) Rhein, V., Song, X., Wiesner, A., Ittner, L. M., Baysang, G., Meier, F., Ozmen, L., Bluethmann, H., Dröse, S., Brandt, U., Savaskan, E., Czech, C., Götz, J., and Eckert, A. (2009) Amyloid-β and Tau Synergistically Impair the Oxidative Phosphorylation System in Triple Transgenic Alzheimer's Disease Mice. *Proc. Natl. Acad. Sci. U. S. A. 106* (47), 20057−20062.
(35) Green, K. N., and LaFerla, F. M. (2008) Linking Calcium to Aβ and Alzheimer's Disease. *Neuron 59*, 190−194.
(36) Gómez-Ramos, A., Díaz-Hernández, M., Rubio, A., Miras-Portugal, M. T., and Avila, J. (2008) Extracellular Tau Promotes Intracellular Calcium Increase through M1 and M3 Muscarinic Receptors in Neuronal Cells. *Mol. Cell. Neurosci. 37* (4), 673−681.
(37) Kawahara, M., and Kuroda, Y. (2000) Molecular Mechanism of Neurodegeneration Induced by Alzheimer's β-Amyloid Protein: Channel Formation and Disruption of Calcium Homeostasis. *Brain Res. Bull. 53*, 389−397.
(38) Oren, O., Ben Zichri, S., Taube, R., Jelinek, R., and Papo, N. (2020) Aβ42 Double Mutant Inhibits Aβ42-Induced Plasma and Mitochondrial Membrane Disruption in Artificial Membranes, Isolated Organs, and Intact Cells. *ACS Chem. Neurosci. 11*, 1027−1037.
(39) Horvath, S. E., and Daum, G. (2013) Lipids of Mitochondria. *Prog. Lipid Res. 52* (4), 590−614.
(40) Fanni, A. M., Vander Zanden, C. M., Majewska, P. V., Majewski, J., and Chi, E. Y. (2019) Membrane-Mediated Fibrillation and Toxicity of the Tau Hexapeptide PHF6. *J. Biol. Chem. 294* (42), 15304−15317.
(41) Ait-Bouziad, N., Lv, G., Mahul-Mellier, A. L., Xiao, S., Zorludemir, G., Eliezer, D., Walz, T., and Lashuel, H. A. (2017) Discovery and Characterization of Stable and Toxic Tau/Phospholipid Oligomeric Complexes. *Nat. Commun. 8*, 1678.
(42) Camilleri, A., Ghio, S., Caruana, M., Weckbecker, D., Schmidt, F., Kamp, F., Leonov, A., Ryazanov, S., Griesinger, C., Giese, A., Cauchi, R. J., and Vassallo, N. (2020) Tau-Induced Mitochondrial Membrane Perturbation Is Dependent upon Cardiolipin. *Biochim. Biophys. Acta, Biomembr. 1862* (2), 183064.
(43) Georgieva, E. R., Xiao, S., Borbat, P. P., Freed, J. H., and Eliezer, D. (2014) Tau Binds to Lipid Membrane Surfaces via Short Amphipathic Helices Located in Its Microtubule-Binding Repeats. *Biophys. J. 107* (6), 1441−1452.
(44) Majewski, J., Jones, E. M., Vander Zanden, C. M., Biernat, J., Mandelkow, E., and Chi, E. Y. (2020) Lipid Membrane Templated

Misfolding and Self-Assembly of Intrinsically Disordered Tau Protein. *Sci. Rep. 10*, 13324.
(45) Marshall, K. E., Morris, K. L., Charlton, D., O'Reilly, N., Lewis, L., Walden, H., and Serpell, L. C. (2011) Hydrophobic, Aromatic, and Electrostatic Interactions Play a Central Role in Amyloid Fibril Formation and Stability. *Biochemistry 50* (12), 2061−2071.
(46) Castelletto, V., Ryumin, P., Cramer, R., Hamley, I. W., Taylor, M., Allsop, D., Reza, M., Ruokolainen, J., Arnold, T., Hermida-Merino, D., Garcia, C. I., Leal, M. C., and Castaño, E. (2017) Self-Assembly and Anti-Amyloid Cytotoxicity Activity of Amyloid Beta Peptide Derivatives. *Sci. Rep. 7*, 43637.
(47) Benbow, S. J., Strovas, T. J., Darvas, M., Saxton, A., and Kraemer, B. C. (2020) Synergistic Toxicity between Tau and Amyloid Drives Neuronal Dysfunction and Neurodegeneration in Transgenic C. Elegans. *Hum. Mol. Genet. 29* (3), 495−505.
(48) Wurth, C., Guimard, N. K., and Hecht, M. H. (2002) Mutations That Reduce Aggregation of the Alzheimer's Aβ42 Peptide: An Unbiased Search for the Sequence Determinants of Aβ Amyloidogenesis. *J. Mol. Biol. 319* (5), 1279−1290.
(49) Korn, A., McLennan, S., Adler, J., Krueger, M., Surendran, D., Maiti, S., and Huster, D. (2018) Amyloid β (1−40) Toxicity Depends on the Molecular Contact between Phenylalanine 19 and Leucine 34. *ACS Chem. Neurosci. 9* (4), 790−799.
(50) Das, A. K., Rawat, A., Bhowmik, D., Pandit, R., Huster, D., and Maiti, S. (2015) An Early Folding Contact between Phe19 and Leu34 Is Critical for Amyloid-β Oligomer Toxicity. *ACS Chem. Neurosci. 6* (8), 1290−1295.
(51) Frenkel-Pinter, M., Richman, M., Belostozky, A., Abu-Mokh, A., Gazit, E., Rahimipour, S., and Segal, D. (2016) Selective Inhibition of Aggregation and Toxicity of a Tau-Derived Peptide Using Its Glycosylated Analogues. *Chem. - Eur. J. 22* (17), 5945−5952.
(52) KrishnaKumar, V. G., Paul, A., Gazit, E., and Segal, D. (2018) Mechanistic Insights into Remodeled Tau-Derived PHF6 Peptide Fibrils by Naphthoquinone-Tryptophan Hybrids. *Sci. Rep. 8*, 71.
(53) Tasi, Y. C., Chin, T. Y., Chen, Y. J., Huang, C. C., Lee, S. L., and Wu, T. Y. (2015) Potential Natural Products for Alzheimer's Disease: Targeted Search Using the Internal Ribosome Entry Site of Tau and Amyloid-β Precursor Protein. *Int. J. Mol. Sci. 16* (4), 8789−8810.
(54) Miller, Y., Ma, B., and Nussinov, R. (2011) Synergistic Interactions between Repeats in Tau Protein and Aβ Amyloids May Be Responsible for Accelerated Aggregation via Polymorphic States. *Biochemistry 50* (23), 5172−5181.
(55) Oren, O., Banerjee, V., Taube, R., and Papo, N. (2018) An Aβ42 Variant That Inhibits Intra- and Extracellular Amyloid Aggregation and Enhances Cell Viability. *Biochem. J. 475* (19), 3087−3103.
(56) Reddy, P. H. (2011) Abnormal Tau, Mitochondrial Dysfunction, Impaired Axonal Transport of Mitochondria, and Synaptic Deprivation in Alzheimer's Disease. *Brain Res. 1415*, 136−148.
(57) Cottrell, D. A., Borthwick, G. M., Johnson, M. A., Ince, P. G., and Turnbull, D. M. (2002) The Role of Cytochrome c Oxidase Deficient Hippocampal Neurones in Alzheimer's Disease. *Neuropathol. Appl. Neurobiol. 28* (5), 390−396.
(58) Halder, S., Yadav, K. K., Sarkar, R., Mukherjee, S., Saha, P., Haldar, S., Karmakar, S., and Sen, T. (2015) Alteration of Zeta Potential and Membrane Permeability in Bacteria: A Study with Cationic Agents. *SpringerPlus 4*, 672.
(59) Mileykovskaya, E., and Dowhan, W. (2009) Cardiolipin Membrane Domains in Prokaryotes and Eukaryotes. *Biochim. Biophys. Acta, Biomembr. 1788*, 2084−2091.
(60) LeVine, H. (1999) Quantification of β-Sheet Amyloid Fibril Structures with Thioflavin T. *Methods Enzymol. 309*, 274−284.
(61) Frenkel-Pinter, M., Richman, M., Belostozky, A., Abu-Mokh, A., Gazit, E., Rahimipour, S., and Segal, D. (2016) Selective Inhibition of Aggregation and Toxicity of a Tau-Derived Peptide Using Its Glycosylated Analogues. *Chem. - Eur. J. 22* (17), 5945−5952.
(62) Jones, E. M., Dubey, M., Camp, P. J., Vernon, B. C., Biernat, J., Mandelkow, E., Majewski, J., and Chi, E. Y. (2012) Interaction of Tau Protein with Model Lipid Membranes Induces Tau Structural Compaction and Membrane Disruption. *Biochemistry 51* (12), 2539−2550.
(63) Zigoneanu, I. G., Yang, Y. J., Krois, A. S., Haque, M. E., and Pielak, G. J. (2012) Interaction of α-Synuclein with Vesicles That Mimic Mitochondrial Membranes. *Biochim. Biophys. Acta, Biomembr. 1818* (3), 512−519.
(64) Malishev, R., Shaham-Niv, S., Nandi, S., Kolusheva, S., Gazit, E., and Jelinek, R. (2017) Bacoside-A, an Indian Traditional-Medicine Substance, Inhibits β-Amyloid Cytotoxicity, Fibrillation, and Membrane Interactions. *ACS Chem. Neurosci. 8* (4), 884−891.
(65) Vestergaard, M., Hamada, T., and Takagi, M. (2008) Using Model Membranes for the Study of Amyloid Beta:Lipid Interactions and Neurotoxicity. *Biotechnol. Bioeng. 99* (4), 753−763.
(66) Brahms, S., and Brahms, J. (1980) Determination of Protein Secondary Structure in Solution by Vacuum Ultraviolet Circular Dichroism. *J. Mol. Biol. 138* (2), 149−178.
(67) Dalmas, B., and Bannister, W. H. (1995) Prediction of Protein Secondary Structure from Circular Dichroism Spectra: An Attempt to Solve the Problem of the Best-Fitting Reference Protein Subsets. *Anal. Biochem. 225* (1), 39−48.
(68) Pebay-Peyroula, E., Dufourc, E. J., and Szabo, A. G. (1994) Location of Diphenyl-Hexatriene and Trimethylammonium-Diphenyl-Hexatriene in Dipalmitoylphosphatidylcholine Bilayers by Neutron Diffraction. *Biophys. Chem. 53* (1−2), 45−56.
(69) Rodrigues, C., Gameiro, P., Prieto, M., and De Castro, B. (2003) Interaction of Rifampicin and Isoniazid with Large Unilamellar Liposomes: Spectroscopic Location Studies. *Biochim. Biophys. Acta, Gen. Subj. 1620* (1−3), 151−159.
(70) Sheynis, T., Friediger, A., Xue, W. F., Hellewell, A. L., Tipping, K. W., Hewitt, E. W., Radford, S. E., and Jelinek, R. (2013) Aggregation Modulators Interfere with Membrane Interactions of B2-Microglobulin Fibrils. *Biophys. J. 105* (3), 745−755.
(71) Schlame, M., Brody, S., and Hostetler, K. Y. (1993) Mitochondrial Cardiolipin in Diverse Eukaryotes: Comparison of Biosynthetic Reactions and Molecular Acyl Species. *Eur. J. Biochem. 212* (3), 727−733.
(72) Pickett, E. K., Herrmann, A. G., McQueen, J., Abt, K., Dando, O., Tulloch, J., Jain, P., Dunnett, S., Sohrabi, S., Fjeldstad, M. P., Calkin, W., Murison, L., Jackson, R. J., Tzioras, M., Stevenson, A., d'Orange, M., Hooley, M., Davies, C., Colom-Cadena, M., Anton-Fernandez, A., King, D., Oren, I., Rose, J., McKenzie, C. A., Allison, E., Smith, C., Hardt, O., Henstridge, C. M., Hardingham, G. E., and Spires-Jones, T. L. (2019) Amyloid Beta and Tau Cooperate to Cause Reversible Behavioral and Transcriptional Deficits in a Model of Alzheimer's Disease. *Cell Rep. 29* (11), 3592−3604.
(73) Huang, A., and Stultz, C. M. (2007) Conformational Sampling with Implicit Solvent Models: Application to the PHF6 Peptide in Tau Protein. *Biophys. J. 92* (1), 34−45.
(74) Barghorn, S., Davies, P., and Mandelkow, E. (2004) Tau Paired Helical Filaments from Alzheimer's Disease Brain and Assembled in Vitro Are Based on-Structure in the Core Domain. *Biochemistry 43*, 1694−1703.
(75) Eckert, A., Schmitt, K., and Gotz, J. (2011) Mitochondrial Dysfunction - The Beginning of the End in Alzheimer's Disease? Separate and Synergistic Modes of Tau and Amyloid-β Toxicity. *Alzheimer's Res. Ther. 3*, 15.
(76) Caughey, B., and Lansbury, P. T. (2003) P ROTOFIBRILS, P ORES, F IBRILS, AND N EURODEGENERATION: Separating the Responsible Protein Aggregates from The Innocent Bystanders. *Annu. Rev. Neurosci. 26* (1), 267−298.
(77) Ross, P. D., and Subramanian, S. (1981) Thermodynamics of Protein Association Reactions: Forces Contributing to Stability. *Biochemistry 20* (11), 3096−3102.
(78) Wang, S. H., Liu, F. F., Dong, X. Y., and Sun, Y. (2010) Thermodynamic Analysis of the Molecular Interactions between

Amyloid β-Peptide 42 and (−)-Epigallocatechin-3-Gallate. *J. Phys. Chem. B 114* (35), 11576−11583.
(79) Van Gils, J. H. M., Van Dijk, E., Peduzzo, A., Hofmann, A., Vettore, N., Schützmann, M. P., Groth, G., Mouhib, H., Otzen, D. E., Buell, A. K., and Abeln, S. (2020) The Hydrophobic Effect Characterises the Thermodynamic Signature of Amyloid Fibril Growth. *PLoS Comput. Biol. 16* (5), e1007767.
(80) Selkoe, D. J., and Hardy, J. (2016) The Amyloid Hypothesis of Alzheimer's Disease at 25 Years. *EMBO Mol. Med. 8* (6), 595−608.
(81) Pascoal, T. A., Mathotaarachchi, S., Shin, M., Benedet, A. L., Mohades, S., Wang, S., Beaudry, T., Kang, M. S., Soucy, J.-P., Labbe, A., Gauthier, S., and Rosa-Neto, P. (2017) Synergistic Interaction between Amyloid and Tau Predicts the Progression to Dementia. *Alzheimer's Dementia 13* (6), 644−653.
(82) Cao, P., and Raleigh, D. P. (2012) Analysis of the Inhibition and Remodeling of Islet Amyloid Polypeptide Amyloid Fibers by Flavanols. *Biochemistry 51* (13), 2670−2683.
(83) Lemkul, J. A., and Bevan, D. R. (2012) Morin Inhibits the Early Stages of Amyloid β-Peptide Aggregation by Altering Tertiary and Quaternary Interactions to Produce "off-Pathway" Structures. *Biochemistry 51* (30), 5990−6009.
(84) Gorsky, M. K., Burnouf, S., Dols, J., Mandelkow, E., and Partridge, L. (2016) Acetylation Mimic of Lysine 280 Exacerbates Human Tau Neurotoxicity in Vivo. *Sci. Rep. 6*, 22685.
(85) Götz, J., Xia, D., Leinenga, G., Chew, Y. L., and Nicholas, H. R. (2013) What Renders TAU Toxic. *Front. Neurol. 4*, 72.
(86) Cheng, Y., and Bai, F. (2018) The Association of Tau with Mitochondrial Dysfunction in Alzheimer's Disease. *Front. Neurosci. 12*, 163.
(87) Hong, L., Huang, H. C., and Jiang, Z. F. (2014) Relationship between Amyloid-Beta and the Ubiquitin-Proteasome System in Alzheimer's Disease. *Neurol. Res. 36*, 276−282.
(88) Liu, J., and Li, L. (2019) Targeting Autophagy for the Treatment of Alzheimer's Disease: Challenges and Opportunities. *Front. Mol. Neurosci. 12*, 203.
(89) Bustamante, H. A., González, A. E., Cerda-Troncoso, C., Shaughnessy, R., Otth, C., Soza, A., and Burgos, P. V. (2018) Interplay between the Autophagy-Lysosomal Pathway and the Ubiquitin-Proteasome System: A Target for Therapeutic Development in Alzheimer's Disease. *Front. Cell. Neurosci. 12*, 126.
(90) Bellia, F., Lanza, V., García-Viñuales, S., Ahmed, I. M. M., Pietropaolo, A., Iacobucci, C., Malgieri, G., D'Abrosca, G., Fattorusso, R., Nicoletti, V. G., Sbardella, D., Tundo, G. R., Coletta, M., Pirone, L., Pedone, E., Calcagno, D., Grasso, G., and Milardi, D. (2019) Ubiquitin Binds the Amyloid β Peptide and Interferes with Its Clearance Pathways. *Chem. Sci. 10* (9), 2732−2742.
(91) Camara, A. K. S., Zhou, Y. F., Wen, P. C., Tajkhorshid, E., and Kwok, W. M. (2017) Mitochondrial VDAC1: A Key Gatekeeper as Potential Therapeutic Target. *Front. Physiol. 8*, 460.
(92) Viswanathan, G., Mohapatra, S., Paul, A., Arad, E., Jelinek, R., Gazit, E., and Segal, D. (2018) Inhibitory Effect of Naphthoquinone-Tryptophan Hybrid towards Aggregation of PAP F39 Semen Amyloid. *Molecules 23* (12), 3279.
(93) Godinot, C., and Gautheron, D. C. (1979) Separation of Right-Side-out and inside-out Submitochondrial Particles by Affinity Chromatography on Sepharose-Cytochrome C. *Methods Enzymol. 55* (C), 112−114.
(94) Berry, E. A., and Trumpower, B. L. (1987) Simultaneous Determination of Hemes a, b, and c from Pyridine Hemochrome Spectra. *Anal. Biochem. 161* (1), 1−15.
(95) ThermoFisher Scientific. (2010) Probes for Lipids and Membranes. *Mol. Probes Handbk. 76* (11), 547−589.
(96) do Canto, A. M. T. M., Robalo, J. R., Santos, P. D., Carvalho, A. J. P., Ramalho, J. P. P., and Loura, L. M. S. (2016) Diphenylhexatriene Membrane Probes DPH and TMA-DPH: A Comparative Molecular Dynamics Simulation Study. *Biochim. Biophys. Acta, Biomembr. 1858* (11), 2647−2661.
(97) Gidwani, A., Holowka, D., and Baird, B. (2001) Fluorescence Anisotropy Measurements of Lipid Order in Plasma Membranes and Lipid Rafts from RBL-2H3 Mast Cells. *Biochemistry 40* (41), 12422−12429.

https://doi.org/10.1021/acschemneuro.1c00045
ACS Chem. Neurosci. 2021, 12, 1563−1577